Quantitative Structural Organization of Bulk Apical Membrane Traffic in Pollen Tubes[1][OPEN]

Gleb Grebnev,[a] Mislav Cvitkovic,[b,c,2] Carolin Fritz,[a] Giampiero Cai,[d] Ana-Suncana Smith,[b,c] and Benedikt Kost[a,3,4]

[a]Cell Biology, Department of Biology, Friedrich-Alexander-University Erlangen Nuremberg, 91058 Erlangen, Germany
[b]PULS Group, Department of Physics, Friedrich-Alexander-University Erlangen Nuremberg, 91058 Erlangen, Germany
[c]Group for Computational Life Sciences, Division of Physical Chemistry, Ruđer Bošković Institute, 10000 Zagreb, Croatia
[d]Department of Life Sciences, University of Siena, 53100 Siena, Italy

ORCID IDs: 0000-0001-9377-9153 (G.G.); 0000-0001-6148-8263 (M.C.); 0000-0001-7514-5747 (C.F.); 0000-0002-4511-3557 (G.C.); 0000-0002-0835-0086 (A.-S.S.); 0000-0003-2249-2555 (B.K.)

Pollen tube tip growth depends on balancing secretion of cell wall material with endocytic recycling of excess material incorporated into the plasma membrane (PM). The classical model of tip growth, which predicts bulk secretion, occurs apically, and is compensated by subapical endocytosis, has been challenged in recent years. Many signaling proteins and lipids with important functions in the regulation of membrane traffic underlying tip growth associate with distinct regions of the pollen tube PM, and understanding the mechanisms responsible for the targeting of these regulatory factors to specific PM domains requires quantitative information concerning the sites of bulk secretion and endocytosis. Here, we quantitatively characterized the spatial organization of membrane traffic during tip growth by analyzing steady-state distributions and dynamics of FM4-64-labeled lipids and YFP-tagged transmembrane (TM) proteins in tobacco (*Nicotiana tabacum*) pollen tubes growing normally or treated with Brefeldin A to block secretion. We established that (1) secretion delivers TM proteins and recycled membrane lipids to the same apical PM domain, and (2) FM4-64-labeled lipids, but not the analyzed TM proteins, undergo endocytic recycling within a clearly defined subapical region. We mathematically modeled the steady-state PM distributions of all analyzed markers to better understand differences between them and to support the experimental data. Finally, we mapped subapical F-actin fringe and trans-Golgi network positioning relative to sites of bulk secretion and endocytosis to further characterize functions of these structures in apical membrane traffic. Our results support and further define the classical model of apical membrane traffic at the tip of elongating pollen tubes.

Pollen tube tip growth is essential for plant reproduction and is widely employed as a model to investigate directional cell expansion in plants, which plays a central role in single-cell as well as organ morphogenesis. Pollen tubes expand very rapidly at rates of several micrometer per minute strictly in one direction based on massive local secretion of cell wall material at the tip (Hepler et al., 2001; Kost, 2008; Yalovsky et al., 2008). The pollen tube cytoplasm displays extreme polarization: poorly characterized cellular and molecular mechanisms are responsible for the massive accumulation of vesicles containing cell wall material within an inverted cone-shaped apical region (apical region of vesicle accumulation [ARVA]), behind which all other cell organelles are located (Lancelle and Hepler, 1992; Derksen et al., 1995; Hepler et al., 2001; Cheung and Wu, 2007). These organelles include a detached trans-Golgi network (TGN) compartment, which, depending on interactions with a subapical cortical F-actin fringe, is stably positioned directly behind the ARVA and may generate the secretory vesicles observed within this region (Stephan et al., 2014). The F-actin fringe is essential for tip growth (Bou Daher and Geitmann, 2011; Dong et al., 2012; Rounds et al., 2014; Stephan et al., 2014), possibly because of additional direct functions in the transport of secretory vesicles (Cárdenas et al., 2008; Bou Daher and Geitmann, 2011; Dong et al., 2012; Rounds et al., 2014) or in local endocytic membrane internalization (Samaj et al., 2006; Galletta and Cooper, 2009; Moscatelli et al., 2012; Meunier and Gutiérrez, 2016; Li et al., 2018). Most other cytoplasmic organelles are rapidly transported along longitudinally oriented F-actin cables back and forth between the two ends of elongating pollen tubes ("cytoplasmic streaming"; Hepler et al., 2001; Cheung and Wu, 2007; Cai et al., 2015).

Cell wall biogenesis at the tip of growing pollen tubes requires secretion at an eight to 10 times higher rate than required for plasma membrane (PM) extension (Picton and Steer, 1983; Derksen et al., 1995; Bove et al., 2008; Ketelaar et al., 2008). Assuming that secretory vesicles completely fuse with the PM rather than delivering their cargo based on temporary "kiss-and-run" fusion, this implies that secretion results in massive

incorporation of excess material into the PM, which needs to be endocytically recycled. "Kiss-and-run" fusion was proposed to occur in neuronal synapses decades ago but has remained controversial, as this process is difficult to experimentally investigate and unequivocally demonstrate (He and Wu, 2007; Alabi and Tsien, 2013). In fact, no experimental evidence for "kiss-and-run" fusion in growing pollen tubes has been reported to date. By contrast, data obtained based on evanescent wave (total internal reflection fluorescence) microscopy strongly support complete fusion of FM4-64 labeled secretory vesicles with the PM of *Picea meyeri* pollen tubes (Wang et al., 2006).

The classical model of pollen tube tip growth (Steer, 1989; Derksen et al., 1995; Kost, 2008) is supported by compelling albeit largely circumstantial evidence and has been challenged in recent years (Grebnev et al., 2017). It predicts that massive secretion required for cell wall biogenesis occurs apically and is compensated by subapical endocytic recycling of excess PM material. In addition to delivering material needed for cell wall construction, massive apical secretion is also proposed to be essential for the coordination of signaling processes regulating tip growth (Luo et al., 2017; Li et al., 2018). As the pollen tube cell wall exclusively expands within the apical dome, it needs to display plasticity within this region paired with sufficient stiffness to prevent cell bursting caused by turgor pressure that drives cell elongation (Bosch et al., 2005; Bosch and Hepler, 2005; Zerzour et al., 2009). Specifically, at the apex, the pollen tube cell wall is primarily composed of methyl-esterified pectins (Bosch et al., 2005), which are synthesized in the Golgi and delivered to the cell surface by secretion (Hepler et al., 2013; Mollet et al., 2013). Extracellular pectin methylesterases (PMEs) as well as inhibitors of these enzymes (PMEIs) are also secreted into the cell wall (Hepler et al., 2013; Mollet et al., 2013). Specific PMEI accumulation at the apex (Röckel et al., 2008) appears to contribute to the restriction of PME-mediated pectin de-esterification, which enhances cell wall stiffness, to lateral regions of the cell wall (Hepler et al., 2013; Mollet et al., 2013).

Fluorescence recovery after photobleaching (FRAP) analysis established that after photobleaching, fluorescence emitted by a secreted PME-GFP fusion protein first recovers within the pollen tube cell wall at the extreme apex before it spreads to more lateral regions (Wang et al., 2013). This observation is supported by in vivo analyses of the delivery of fluorescent proteins fused to the receptor-like kinase POLLEN RECEPTOR-LIKE KINASE1 (AtPRK1), a transmembrane (TM) protein with an extracellular ligand binding domain, through the secretory endomembrane system to the PM at the pollen tube tip (Lee et al., 2008; Luo et al., 2016). After photobleaching or photoactivation, PM-associated fluorescence emitted by AtPRK1 fusion proteins also first appears at the extreme apex, indicating that not only the delivery of extracellular proteins to the cell wall but also the transport of TM proteins to the PM may be mediated by apical secretion. However, PMEs and AtPRK1 both contain extracellular domains that may interact with cell wall components specifically at the apex. Therefore, these proteins may be subapically secreted and subsequently recruited to the pollen tube apex by specific interactions with cell wall components (McKenna et al., 2009).

Coated pits, sites of clathrin-mediated endocytosis, are enriched within the subapical PM of fixed or living pollen tubes, as demonstrated by numerous studies based on transmission electron microscopy (TEM; Derksen et al., 1995), immunofluorescence, and fluorescent protein tagging (Blackbourn and Jackson, 1996; Zhao et al., 2010; Feng et al., 2016; Sekereš et al., 2017; Li et al., 2018; Muro et al., 2018; Kaneda et al., 2019). Consistent with these observations, endocytosed externally applied fluorescent lipid dyes (FM4-64; Parton et al., 2001) or positively charged nanogold particles (Moscatelli et al., 2007) were first detected within cytoplasmic vesicles specifically beneath the subapical PM using fluorescence microscopy or TEM, respectively. At a later stage, both markers are not only observed within endocytic compartments (late endosomes, vacuoles), but also within Golgi stacks and/or apical vesicles. These observations suggest that bulk endocytosis occurs subapically, and that material internalized through this process is partially recycled to the secretory endomembrane system. However, massive endocytosis may also occur at the pollen tube apex based on (1) TEM analysis of the endocytic uptake of nanoparticles carrying a negative rather than a positive (see above) charge (Moscatelli et al., 2007), (2) time-lapse fluorescence imaging of FM4-64 internalization into pollen tubes preloaded with FM1-43 (Zonia and

[1]This work was supported by the German Research Foundation within the framework of the Research Training Group 1962 (projects nos. RTG 1962 7 to G.G. and B.K. and RGT 1962 10 to M.C. and A.-S.S.), the European Research Council StG MembranesAct (grant no. 2013–33728 to M.C. and A.-S.S.), and German Research Foundation Major Equipment Grants (grant nos. INST90/1074–1FUGG [for SP8 DIVE-FALCON microscope] and INST90/1025–1FUGG [for plant growth chamber facility for tobacco] to B.K.).

[2]Present address: Department of Physics, University of Split, 21000 Split, Croatia

[3]Author for contact: benedikt.kost@fau.de.

[4]Senior author.

The author responsible for distribution of materials integral to the findings presented in this article in accordance with the policy described in the Instructions for Authors (www.plantphysiol.org) is: Benedikt Kost (benedikt.kost@fau.de).

G.G. acquired most of the experimental data and contributed to the design of the experiments, to the analysis and interpretation of experimental data, as well as to the writing of the manuscript; C.F. contributed all long-term time lapse imaging data; M.C. and A.-S.S. developed, analyzed, and interpreted the mathematical model and contributed to the writing of the manuscript; G.C. participated in the characterization of F-actin and TGN functions in membrane traffic; B.K. conceived and administered the study, was responsible for data analysis/interpretation, and wrote the final version of the manuscript.

[OPEN]Articles can be viewed without a subscription.

www.plantphysiol.org/cgi/doi/10.1104/pp.20.00380

Munnik, 2008), and (3) the investigation of mobility patterns of cytoplasmic components within the apical ARVA using differential interference contrast light microscopy or FRAP analysis after FM1-43 staining (Bove et al., 2008).

Many signaling proteins and lipids with important functions in the control of membrane traffic during tip growth are specifically associated with strikingly distinct apical or lateral PM domains not only in pollen tubes, but also in other tip-growing plant cells. These proteins and lipids include (1) RHO-OF-PLANTS (ROP) GTPases (Lin et al., 1996; Sun et al., 2015), (2) upstream regulators of ROP activity (ROP-GAPs [GTPase-activating proteins; Klahre and Kost, 2006] and ROP-GEFs [guanine nucleotide exchange factors; Gu et al., 2006; Le Bail et al., 2019]), (3) different signaling lipids (phosphatidylinositide 4,5-bisphosphate [Kost et al., 1999], diacyl glycerol [Helling et al., 2006], and phosphatidic acid [Potocký et al., 2014]), as well as (4) lipid modifying enzymes (phospholipase C [Dowd et al., 2006; Helling et al., 2006] and PIP5Ks [phosphatidylinositide 4-phosphate 5-kinases; Sousa et al., 2008; Stenzel et al., 2012]). The targeting of these signaling proteins and lipids to specific PM domains in tip-growing cells appears to be essential for the regulation of local secretion and endocytosis but clearly also depends on these membrane transport processes. A thorough understanding of the mechanisms, which target these factors to distinct PM domains and therefore play an essential role in the control of tip growth, clearly requires quantitative characterization of the spatial organization of apical membrane traffic.

A key aim of the study presented here was to quantitatively determine sites of bulk secretion and endocytic membrane recycling required for apical cell wall biogenesis at the tip of growing tobacco (*Nicotiana tabacum*) pollen tubes. To this end, the lipid dye FM4-64 as well as different enhanced yellow fluorescent protein (eYFP)-tagged TM proteins, including proteins unlikely to interact with the cell wall, were employed as in vivo markers. Using fluorescence microscopy, steady-state distributions and dynamic behavior of these markers were characterized in normally growing and/or in Brefeldin A (BFA)-treated tobacco pollen tubes. In addition, to achieve a better understanding of remarkable differences in the observed steady-state distribution patterns of some of the analyzed markers, these patterns were mathematically modeled based on experimental data obtained. Finally, using eYFP-based markers, subapical F-actin fringe and TGN positioning was quantitatively mapped to further characterize functions of these structures in apical vesicle accumulation and membrane traffic. Together, experimental and theoretical data generated (1) quantitatively define sites of bulk secretion and endocytosis within apical and subapical PM regions at the tip of tobacco pollen tubes, respectively; (2) establish the exact subapical positions of the cortical F-actin fringe and of a detached TGN compartment relative to these sites; (3) demonstrate that within the identified subapical region of bulk endocytosis, constitutive recycling of membrane lipids occurs, which generally excludes TM proteins and appears to depend on the subapical TGN compartment but not on the F-actin fringe; and (4) suggest particularly slow diffusion of TM proteins and lipids with the apical region of bulk secretion, a finding that warrants further investigation.

RESULTS

Different TM Proteins Serving as In Vivo Markers for Membrane Traffic Display Distinct Steady-State Distribution Patterns in Tobacco Pollen Tubes

Three different TM proteins, which are transported through the secretory endomembrane system to the PM (endoplasmic reticulum [ER] > Golgi > TGN > secretory vesicles), were fused to an eYFP and used as markers to investigate membrane traffic at the tip of tobacco pollen tubes. To enable the discovery of general principles underlying this process in addition to marker-specific targeting mechanisms, the following TM proteins with highly diverse characteristics were selected: NtINT4, AtRCI2a, and AtPRK1. INOSITOL TRANSPORTER4 (NtINT4) is an endogenous tobacco pollen tube inositol transporter closely related to AtINT4 (Schneider et al., 2006), is composed of 582 amino acids and contains 12 TM domains (Fig. 1A). By contrast, RARE COLD-INDUCIBLE PROTEIN2A (AtRCI2a) is a small 54-amino acid Arabidopsis (*Arabidopsis thaliana*) protein containing only two TM domains that are connected via a very short (6 amino acid) linker and are positioned between even shorter N- and C-terminal extensions (5 and 2 amino acids, respectively; Fig. 1A). Although AtRCI2a functions are poorly understood to date (Capel et al., 1997; Medina et al., 2001), this protein is commonly used as a noninvasive PM marker in plants (Cutler et al., 2000; Serna, 2005; Thompson and Wolniak, 2008). Finally, AtPRK1 is a 662 amino acid Arabidopsis pollen tube receptor-like kinase (RLK) that contains a single central TM domain, which separates an N-terminal extracellular Leu-rich repeat (LRR) ligand-binding domain from an intracellular protein kinase domain (Fig. 1A). The closely related RLK AtPRK2 (96% sequence identity at the amino acid level) plays an important role in the control of ROP signaling in pollen tubes (Zhang and McCormick, 2007; Chang et al., 2013; Zhao et al., 2013; Miyawaki and Yang, 2014). Fluorescent AtPRK1 fusion proteins have previously been employed to investigate apical membrane dynamics in tobacco (Lee et al., 2008) and Arabidopsis (Luo et al., 2016) pollen tubes. To generate fluorescent markers for membrane traffic, eYFP was attached to a predicted cytoplasmic terminus of each of the three selected proteins (NtINT4 and AtPRK1, C terminus; AtRCI2a, N terminus; Thompson and Wolniak, 2008), of which only AtPRK1 contains an N-terminal ER-import signal peptide (SP; Fig. 1A).

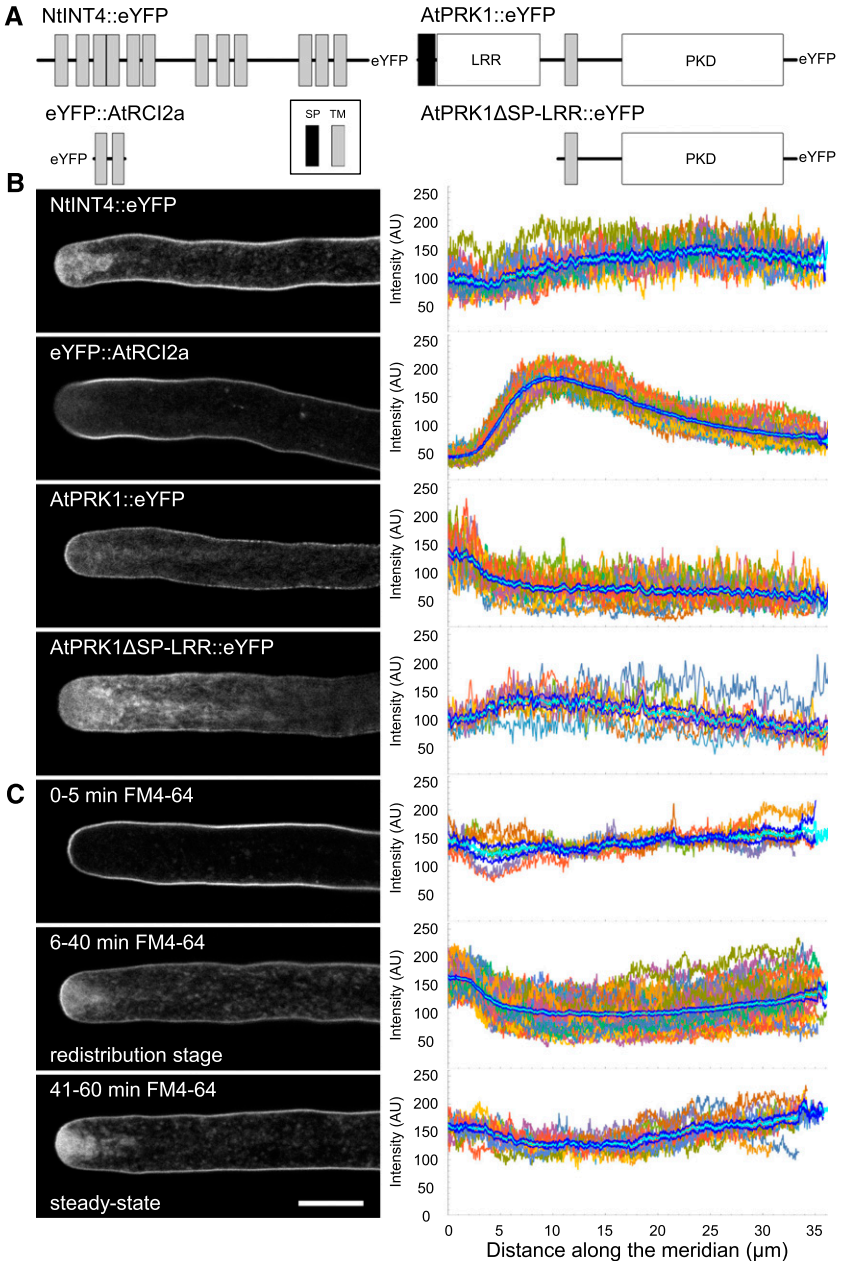

Figure 1. Distribution patterns of TM proteins and FM4-64 serving as markers for membrane traffic in normally growing tobacco pollen tubes. A, Domain structure of the indicated TM protein markers. Protein and domain sizes are drawn to scale. PKD, Protein kinase domain. B, Left, medial confocal optical sections through representative pollen tubes transiently (NtINT4::eYFP, AtPRK1::eYFP or AtPRK1ΔSP-LRR::eYFP) or stably (eYFP::AtRCI2a) expressing the indicated TM protein marker. Growth rates of the individual pollen tubes shown (after confocal imaging): 6.8 μm min^{-1} (NtINT4::eYFP), 3.6 μm min^{-1} (eYFP::AtRCI2a), 3.8 μm min^{-1} (AtPRK1::eYFP), or 4.8 μm min^{-1} (AtPRK1ΔSP-LRR::eYFP). Right, line plots displaying the intensity of PM-associated eYFP fluorescence at different meridional distances from the apex (x = 0 μm) in analyzed pollen tubes (n = 17 [NtINT4::eYFP, three independent experiments], 29 [eYFP::AtRCI2a, five independent experiments], 31 [AtPRK1::eYFP, five independent experiments], or 37 [AtPRK1ΔSP-LRR::eYFP, five independent experiments]). C, Left, medial confocal optical sections through different representative pollen tubes labeled with the fluorescent lipophilic dye FM4-64 (applied at 50 μM in 200 μL PTNT) for the indicated time period (initial stage, 0–5 min; redistribution stage, 6–40 min; steady-state stage, 41–60 min). Growth rates of the individual pollen tubes shown (after confocal imaging): 3.4 μm min^{-1} (0–5 min), 4.8 μm min^{-1} (6–40 min), or 3.8 μm min^{-1} (41–60 min). Right, line plots displaying the intensity of PM-associated FM4-64 fluorescence at different meridional distances from the apex (x = 0 μm) in all analyzed pollen tubes (n = 6 [0–5 min], 68 [6–40 min], or 41 [41–60 min]; four independent experiments). Light blue lines, Average intensity; dark blue lines, SD; all other lines, individual line plots. Scale bar = 10 μm.

Steady-state distribution patterns of NtINT4::eYFP, eYFP::AtRCI2a, and AtPRK1::eYFP transiently or stably expressed under the control of the LAT52 promoter (Twell et al., 1990) in cultured tobacco pollen tubes were imaged using confocal microscopy (Fig. 1B). Only images of normally growing pollen tubes that after confocal imaging continued to elongate at a rate of at least 3 μm min^{-1} (Supplemental Fig. S1A; Klahre and Kost, 2006; Sun et al., 2015; Montes-Rodriguez and Kost, 2017) are shown (Fig. 1B, left) and were statistically analyzed to generate line plots displaying average intensities of PM-associated eYFP fluorescence at different meridional distances (measured along the curved pollen tube PM) from the apex (Fig. 1B, right).

As expected, all three TM protein markers primarily labeled the PM as well as the inverted cone-shaped cytoplasmic ARVA (Lancelle and Hepler, 1992; Derksen et al., 1995; Bove et al., 2008). However, interestingly, the three markers displayed clearly distinct distribution patterns within the PM (Fig. 1B, right), as well as equally clear differences in the relative intensity of PM versus apical vesicle labeling (Fig. 1B, left). Whereas NtINT4::eYFP labeled all regions of the PM as well as apical vesicles essentially evenly, eYFP::AtRCI2a accumulated to highest levels in a lateral PM domain (Stephan et al., 2014), and AtPRK1::eYFP was strongly enriched in the PM within the apical dome as previously described (Lee et al., 2008). Interestingly,

the apical PM domain most strongly labeled by AtPRK1::eYFP extended to a subapical region spanning a meridional distance of about 3 to 5 μm from the extreme apex ($x = 0$ μm), within which the level of PM association of all other markers also appears to markedly change or to display noticeable discontinuity (Fig. 1B).

Differences in the dynamic behavior of each of the three analyzed TM protein makers, which may be caused in part by differential interactions with unequally distributed membrane or cell wall components (Martinière et al., 2012; Trimble and Grinstein, 2015), presumably contribute to the distinct distribution patterns displayed by these makers. In fact, a truncated AtPRK1ΔSP-LRR::eYFP fusion protein, which was missing the entire N terminus of AtPRK1 (amino acids 1–229) including the SP and the extracellular LRR ligand-binding domain (Fig. 1A), displayed an essentially even distribution in the PM and in apical vesicles similar to NtINT4::eYFP (Fig. 1B). This strongly suggests that specific interactions of the LRR domain with the apical cell wall, which by contrast to all other regions of the pollen tube cell wall is mostly composed of esterified pectin (Geitmann and Parre, 2004; Bosch et al., 2005; Parre and Geitmann, 2005; Röckel et al., 2008; Chebli et al., 2012), may be responsible for the observed specific accumulation of full-length AtPRK1::eYFP within the PM at the apex. In the absence of the N-terminal SP of full-length AtPRK1 (Fig. 1A), the TM domain of AtPRK1ΔSP-LRR::eYFP appears to mediate ER recruitment and subsequent membrane insertion of this truncated fusion protein (Shao and Hegde, 2011; Kim and Hwang, 2013).

In addition to differential interactions with membrane or cell wall components, differences in the rates of (1) intramembrane diffusion, which depends on protein size, density and number of TM domains (Saffman et al., 1975; Kusumi et al., 1993; Frick et al., 2007; Goose and Sansom, 2013; Weiß et al., 2013), (2) exocytosis, (3) endocytic uptake, and/or (4) degradation may also contribute to the distinct distribution patterns displayed by the three analyzed markers. These possibilities were further explored by additional experiments and theoretical modeling as described below.

FRAP Analyses of the Dynamic Behavior of TM Protein Markers for Membrane Traffic Demonstrate Apical Secretion

To identify major sites of secretion, at which TM proteins are incorporated into the PM, FRAP analysis was employed to investigate the dynamic behavior of NtINT4::eYFP, eYFP::AtRCI2a, and AtPRK1::eYFP at the tip of growing pollen tubes. After complete photobleaching of eYFP fluorescence at the tip of transiently or stably transformed pollen tubes expressing each of these markers, fluorescence recovery was observed by time-lapse confocal imaging of individual pollen tubes (Fig. 2). PM labeling by all three markers first recovered in the same region within the apical dome 30 to 49 s after photobleaching (Fig. 2, A, third row arrowheads, and B), before the typical steady-state distributions of each of the markers were largely re-established after about 120 s (Fig. 2, fourth row). Interestingly, the apical PM region, in which labeling by all markers first recovered, appears to largely overlap with the membrane domain displaying highest levels of steady-state AtPRK1::eYFP labeling (0 to ~3 μm meridional distance from the extreme apex; Fig. 1B). Larger sets of confocal time-lapse images showing fluorescence recovery in each of the pollen tubes displayed in Figure 2 at higher time resolution are provided as supplemental data (Supplemental Figs. S2–S4). All analyzed pollen tubes grew normally at rates of at least 3 μm min^{-1} during postbleach time-lapse imaging (t = 0 to 116–124 s; Supplemental Fig. S5).

Interestingly, substantial fluorescence recovery was not observed within lateral regions of the PM (more than about 3 μm meridional distance from the extreme apex), which were photobleached together with the apical dome (Fig. 2, A, third and fourth row asterisks, and B). To investigate this more thoroughly, large regions of NtINT4::eYFP-, eYFP::AtRCI2a-, or AtPRK1::eYFP-expressing pollen tubes positioned just behind the apical dome were completely photobleached. In these experiments, even after an extended postbleach period of 360 s, very little recovery of PM-associated fluorescence was observed within the bleached regions (Supplemental Fig. S6, A, third row asterisks, and B) although all analyzed pollen tubes grew normally at rates of at least 3 μm/min during postbleach time-lapse imaging (t = 0 to 360 s; Supplemental Fig. S7). Furthermore, in control experiments NtINT4::eYFP-, eYFP::AtRCI2a- or AtPRK1::eYFP-expressing pollen tubes were preincubated with BFA, a drug that disrupts membrane traffic and blocks tip growth (Supplemental Fig. S8), before they were completely photobleached at the tip. These experiments showed that BFA treatment effectively prevented recovery of apical PM labeling by each of these markers (Supplemental Fig. S9) in all analyzed pollen tubes. Together, these observations demonstrate that after photobleaching, rapid and effective recovery of PM labeling by fluorescent TM protein markers is confined to a small region within the apical dome and depends on active membrane traffic.

In summary, the results presented in this section establish that three different TM proteins serving as markers for membrane traffic are specifically delivered to the same small PM domain within the apical dome of normally growing pollen tubes, strongly suggesting that this PM domain represents a major site of secretion.

Analysis of the Establishment of Steady-State PM Labeling by FM4-64, a Fluorescent Lipid Marker for Membrane Traffic, Supports Apical Secretion

As described in the literature, the fluorescent lipophilic dye FM4-64 becomes red fluorescent upon incorporation into the pollen tube PM and is subsequently

endocytosed (Parton et al., 2001, 2003; Bolte et al., 2004; van Gisbergen et al., 2008). Consistent with the requirement of pollen tube tip growth for massive membrane recycling (see "Introduction"), a large proportion of the endocytosed FM4-64-labeled PM material is rapidly recycled back to the secretory endomembrane system, whereas only a small proportion of this material enters the endocytic endomembrane system and eventually (about 24 h after dye application) detectably labels endosomal and vacuolar compartments (Parton et al., 2001).

Confocal time course imaging was performed to carefully investigate changes in FM4-64 labeling patterns

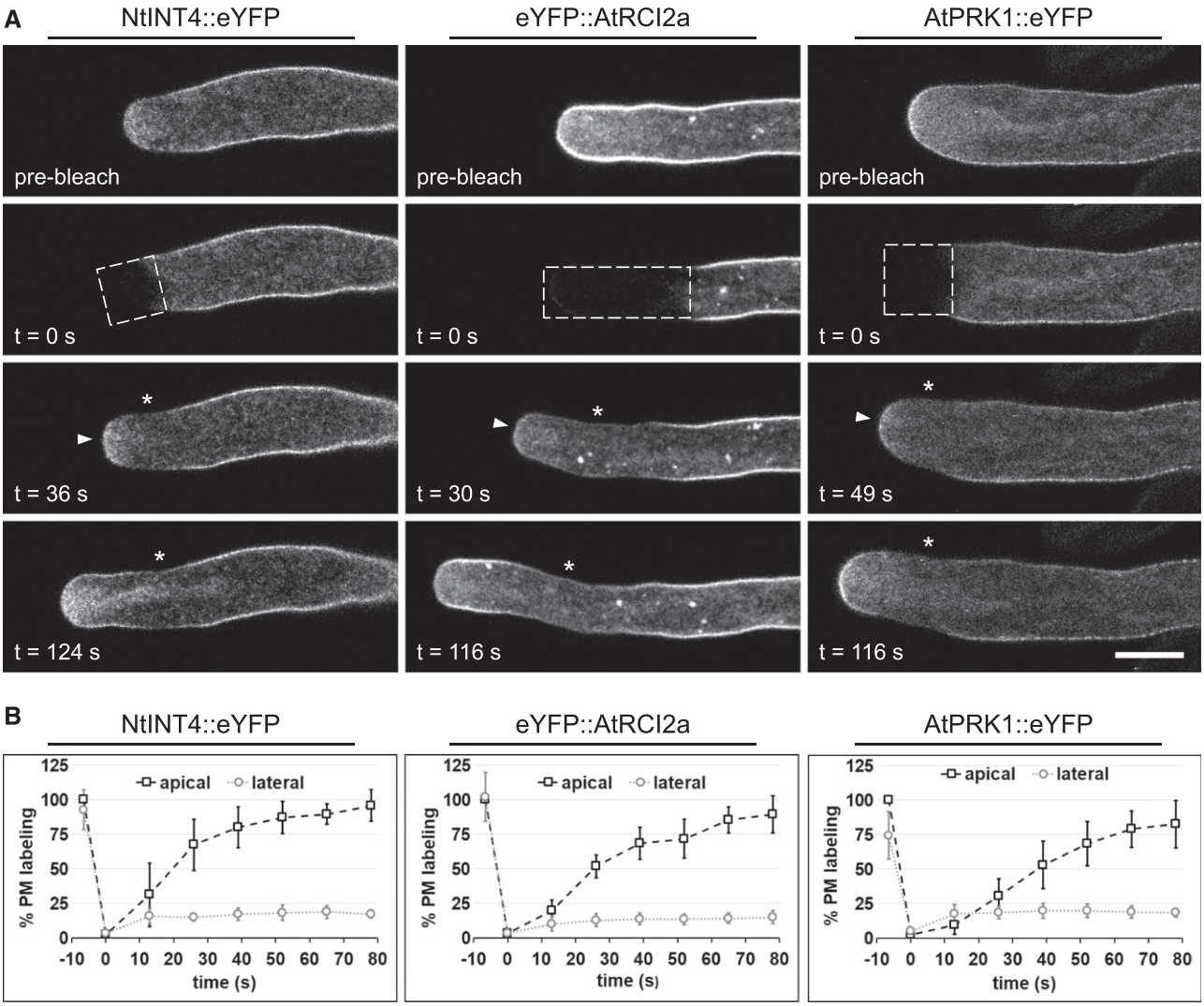

Figure 2. FRAP time-lapse analysis of TM protein marker dynamics at the tip of normally growing tobacco pollen tubes. A, Medial confocal optical sections through representative pollen tubes transiently (NtINT4::eYFP or AtPRK1::eYFP) or stably (eYFP::AtRCI2a) expressing the indicated TM protein marker, which were recorded before (row 1, prebleach) or after complete photobleaching of eYFP fluorescence within the dashed box indicated in row 2. t, Time elapsed after photobleaching; arrowheads, apical PM domain within which fluorescence recovery was first observed; *, bleached lateral PM domain showing no fluorescence recovery. Scale bar = 10 μm. During postbleach time-lapse imaging (t = 0 to 116–124 s), the growth rate of the individual pollen tubes shown was 4.2 μm min^{-1} (NtINT4::eYFP), 8.7 μm min^{-1} (eYFP::AtRCI2a), and 5.1 μm min^{-1} (AtPRK1::eYFP). In total, seven (NtINT4::eYFP, two independent experiments), 10 (eYFP::AtRCI2a, two independent experiments), or 12 (AtPRK1::eYFP, three independent experiments) TM protein-marker-expressing pollen tubes were analyzed. Each TM protein marker displayed essentially the same fluorescence recovery pattern and kinetics in all analyzed pollen tubes. B, Quantification of PM labeling by the indicated TM protein marker in the bleached region either at the extreme apex (0 μm meridional distance from the extreme apex; arrowheads in A; open squares) or in the center of a lateral domain (more than 3 μm meridional distance from the extreme apex; asterisks in A; open circles) immediately before (t = −6.5 s) and after (t = 0 s) photobleaching, as well as after different recovery periods (13, 26, 39, 52, 65, and 78 s). The indicated average levels of PM labeling were computed from data obtained from all analyzed pollen tubes (A) after normalization based on prebleach levels of PM labeling at the extreme apex, which were set to 100%.

during the first 60 min after dye application to cultured tobacco pollen tubes (Fig. 1C). Immediately after application (0–5 min), FM4-64 exclusively and evenly labeled the PM (Fig. 1C, first row). Subsequently, dye redistribution was observed as a consequence of membrane traffic, which resulted about 40 min after dye application in the establishment of a steady-state labeling pattern that remained stable for the rest of the observation period (41–60 min). At this steady-state stage, FM4-64 specifically and evenly labeled not only the PM but also apical vesicles (Fig. 1C, third row). These observations are consistent with data reported in the literature (Parton et al., 2001). However, particularly informative was the imaging of pollen tubes 6 to 40 min after FM4-64 application, during which dye redistribution resulting from endocytic uptake and recycling to the secretory endomembrane system was observed. At this dye redistribution stage, which was not carefully investigated in previous studies, FM4-64 most strongly labeled a small PM domain within the apical dome (Fig. 1C, second row). Interestingly, this domain appeared to largely overlap with the apical membrane region, which displays steady-state AtPRK1::eYFP accumulation at highest levels (0 to ~3 μm meridional distance from the extreme apex; Fig. 1B), and in which labeling by all TM protein markers first recovered in FRAP time-lapse experiments (Fig. 2). Figure 1C shows images of normally growing pollen tubes (Fig. 1C, left) that after confocal imaging continued to elongate at a rate of at least 3 μm min^{-1} (Supplemental Fig. S1B), along with line plots displaying average intensities of PM-associated eYFP fluorescence in such pollen tubes at different meridional distances from the apex (Fig. 1C, right). A larger set of time course images showing changing FM4-64 labeling patterns during the first 60 min after dye application at higher time resolution is provided as supplemental data (Supplemental Fig. S10). Essentially, the same changes in the FM4-64 labeling pattern during this time period were also observed by time lapse imaging of individual pollen tubes (Supplemental Fig. S11A).

Results discussed in the previous paragraph establish that in normally elongating pollen tubes, the steady-state distributions of externally applied FM4-64 (Fig. 1C, third row; Supplemental Fig. S11A, right) and of endogenously produced TM protein markers (Fig. 1B), in particular of NtINT4::eYFP and AtPRK1ΔSP-LRR::eYFP, were remarkably similar. This underscores the usefulness of FM4-64 and of the analyzed TM protein markers as excellent tools to investigate major routes of apical trafficking of PM-associated lipids and proteins, respectively, during pollen tube tip growth. Furthermore, the preferential accumulation of FM4-64 in a small PM region within the apical dome at the dye redistribution stage (6–40 min after application; Fig. 1C, center row; Supplemental Fig. S11A, center) strongly suggests that PM-associated FM4-64 is actively transported from sites of endocytic internalization to the apical major site of secretion, which was identified based on FRAP analyses of the dynamic behavior of TM protein markers (Fig. 2) and also displayed highest levels of steady-state AtPRK1::eYFP accumulation (Fig. 1B). Continued endocytic FM4-64 internalization and recycling during the dye redistribution stage appears to cause increasing dye saturation of apical vesicles, eventually resulting in even labeling of these vesicles and of the PM at the steady-state stage. Based on this interpretation, changes in FM4-64 labeling patterns observed during the first 60 min after dye application further support the identification of a small PM region within the apical dome as a major site of secretion and indicate that membrane traffic results in the massive delivery not only of proteins but also of recycled lipid components of the PM to this site.

Analysis of BFA-Induced Loss of FM4-64 PM Labeling Demonstrates Subapical Endocytosis of PM Lipids

As discussed perviously, BFA blocks pollen tube tip growth (Supplemental Fig. S8) by disrupting membrane traffic. More specifically, in plants, a key effect of BFA treatment is the inhibition of the formation of exocytic vesicles at the TGN (Geldner et al., 2001; Nebenführ et al., 2002), which in these organisms is not only a key component of the secretory endomembrane system, but also serves as an early and recycling endosome (Dettmer et al., 2006; Lam et al., 2007; Reyes et al., 2011; Contento and Bassham, 2012; Paez Valencia et al., 2016). By contrast, endocytic uptake of PM material continues in the presence of BFA (Baluska et al., 2002; Emans et al., 2002; Wang et al., 2005). Consequently, in different types of plant cells (Geldner et al., 2001; Parton et al., 2001, 2003), including tobacco pollen tubes (Helling et al., 2006; Röckel et al., 2008; Stephan et al., 2014), BFA blocks the recycling of endocytosed material back to the PM and causes this material to be trapped within the TGN. BFA effects on growing pollen tubes have been reported to take about 20 min to fully develop (Parton et al., 2001, 2003; Rounds et al., 2014). This drug generally induces aberrant TGN elements to fuse to so-called BFA compartments (Lippincott-Schwartz et al., 1991; Nebenführ et al., 2002; Tse et al., 2006), which in pollen tubes typically form a single subapical structure that becomes detectable only after prolonged (≥30–60 min) incubation (Parton et al., 2001, 2003; Helling et al., 2006; Stephan et al., 2014).

Based on the known BFA effects summarized in the previous paragraph, we hypothesized that BFA treatment of pollen tubes displaying FM4-64 labeling (Fig. 1C) should result in a reduction of PM labeling selectively at major sites of endocytic uptake of membrane material. In fact, this was observed by confocal time course imaging of FM4-64 fluorescence displayed by cultured tobacco pollen tubes, which had been grown for 30 min in the presence of FM4-64 (dye redistribution stage; Fig. 1C, second row), before the dye was washed out from the culture medium and BFA was added (Fig. 3, A and B). Whereas the PM remained essentially evenly labeled for the first 20 min after BFA

application, during the following 20 min, PM-associated FM4-64 fluorescence selectively decreased slightly within the apical dome and massively within a sharply defined subapical region. Interestingly, 41 to 60 min after BFA application, FM4-64 labeling of the PM within the apical dome further decreased to almost the same level as observed within this subapical region (Fig. 3, A and B). A BFA compartment was often not clearly discernible in the analyzed pollen tubes, as strong FM4-64 labeling of this compartment typically only starts to develop after 30 to 60 min in the presence of BFA (Parton et al., 2001, 2003). Figure 3A shows representative images of different FM4-64-labeled pollen tubes recorded during the indicated time periods after BFA application. A larger set of time course images showing changes in FM4-64 distribution in BFA-treated pollen tubes at higher time resolution is provided as supplemental data (Supplemental Fig. S12). Essentially the same changes in FM4-64 labeling patterns within the first 60 min after BFA application were also observed by time-lapse imaging of individual pollen tubes (Supplemental Fig. S11B, first row). Figure 3B shows

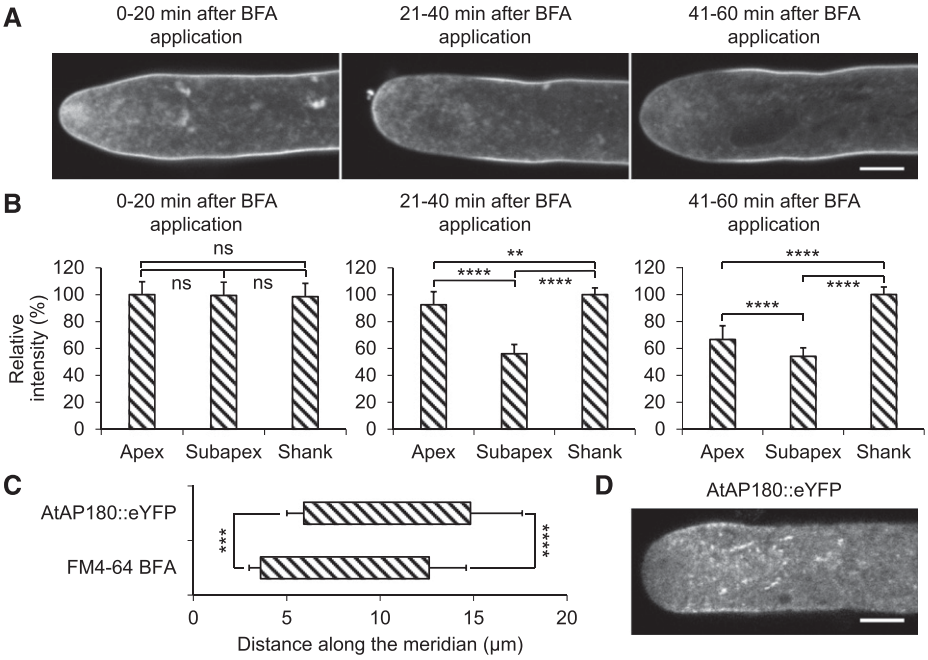

Figure 3. Time course analysis of BFA-induced loss of FM4-64 PM labeling and investigation of AtAP180::eYFP distribution in tobacco pollen tubes. A, Medial confocal optical sections through different representative pollen tubes, which were grown in the presence of FM4-64 (applied at 50 μM in 200 μL PTNT) for 30 min, before the dye was washed out from the culture medium and BFA was applied for the indicated time period (70 μM in 200 μL PTNT). Scale bar = 5 μm. As a result of the BFA treatment, tip growth of all analyzed pollen tubes was completely inhibited (Supplemental Fig. S8). All pollen tubes analyzed during each time period after BFA application (n = 10 [0–20 min], 22 [21–40 min], and 35 [41–60 min]; three independent experiments) displayed very similar FM4-64 labeling patterns. B, Quantitative analysis of the average relative intensity of PM-associated FM4-64 fluorescence in all pollen tubes analyzed as described in A within the apical dome (Apex, meridional distance from the apex, 0–3.6 μm), within a subapical region displaying massive loss of FM4-64 PM labeling in the presence of BFA (Subapex, meridional distance from the apex, 3.6–12.6 μm), and in the shank (Shank, meridional distance from the apex, 12.6–32.6 μm). The borders between these three PM regions were determined as described in C. The intensity of PM-associated FM4-64 fluorescence was normalized in each analyzed pollen tube based on the highest measured value (0–32.6 μm meridional distance from the apex), which was set to 100%. The statistical significance of differences in the average intensity of PM-associated FM4-64 fluorescence between the three different PM regions during each time period after BFA application was assessed using ANOVA (Tukey's test, one way; $^{**}P \leq 0.01$ and $^{****}P \leq 0.0001$; ns, not significantly different [$P > 0.05$]). Error bars = SD. C, Quantitative analysis of the exact length and position of the subapical PM domains, which displayed massive loss of FM4-64 PM labeling 21 to 40 min after BFA application (A) or were associated with an AtAP180::eYFP fusion protein serving as a marker for sites of clathrin-mediated endocytosis (D). The average meridional distances from the extreme apex (x = 0) of both ends of these domains in all analyzed pollen tubes (n = 22 [FM4-64 BFA] or 22 [AtAP180::eYFP]) are indicated. Exact extensions of domains shown: 5.9 ± 0.91 to 14.8 ± 2.8 μm (AtAP180::eYFP); 3.6 ± 0.61 to 12.6 ± 2.0 μm (FM4-64 BFA). The statistical significance of differences between the average meridional distances of both the proximal and the distal ends of the FM4-64 BFA and AtAP180::eYFP domains was assessed using a Student's t test (two-tailed, type II; $^{***}P \leq 0.001$ and $^{****}P \leq 0.0001$). Error bars = SD. D, Medial confocal optical section through a representative normally growing pollen tube transiently expressing an AtAP180::eYFP fusion protein that serves as a marker for sites of clathrin-mediated endocytosis. In total, 25 essentially normally growing pollen tubes were analyzed in two independent experiments, which displayed very similar AtAP180::eYFP distribution patterns. Growth rate of the pollen tube shown (after confocal imaging): 4.8 μm min^{-1}. Scale bar = 5 μm.

the results of a quantitative and statistical analysis of changes in the intensity of PM-associated FM4-64 fluorescence in all pollen tubes analyzed by time course imaging in the apical dome, the subapical region and the shank. Furthermore, the exact average length and position of the subapical region displaying massive loss of PM-associated fluorescence 21 to 40 min after BFA application was determined in these pollen tubes (Fig. 3C; FM4-64 BFA).

In summary, data presented in Figure 3, A, B, and C, as well as in Supplemental Figure S11B, identify a subapical region of the tobacco pollen tube PM as a major site of endocytic uptake of FM4-64-labeled lipid material. This region extends between proximal and distal ends positioned at an average meridional distance of 3.6 and 12.6 μm, respectively, from the extreme apex ($x = 0$ μm). Ongoing endocytic uptake massively reduces FM4-64 labeling of the PM within this region 21 to 40 min after BFA treatment, apparently because this drug blocks recycling of internalized dye via the secretory endomembrane system back to the apical PM. The delayed massive reduction of PM labeling also within the apical dome 41 to 60 min after BFA treatment appears to be caused by FM4-64 diffusion from this PM domain to the subapical major site of endocytosis followed by dye internalization at this site. By contrast, a reduction of FM4-64 labeling of the PM in the shank was not detected within 60 min after BFA application, presumably because the dye pool in this region of the PM was much larger.

The PM Association Pattern of AtAP180::eYFP, a Marker for Clathrin-Mediated Endocytosis at the PM, Supports Subapical Endocytosis

AtAP180 is a component of the clathrin machinery (Barth and Holstein, 2004), which is required for the formation of endocytic vesicles at the PM during clathrin-mediated endocytosis, the most prominent form of endocytosis in plants (Dhonukshe et al., 2007; Pérez-Gómez and Moore, 2007; Fan et al., 2015). Fluorescent AtAP180 fusion proteins have been employed to identify endocytic PM domains in different types of cells, including tobacco pollen tubes (Stavrou and O'Halloran, 2006; Zhao et al., 2010; Kaneda et al., 2019). Consistent with previously reported observations (Zhao et al., 2010; Kaneda et al., 2019), confocal imaging of essentially normally growing tobacco pollen tubes transiently expressing an AtAP180::eYFP fusion protein established that this fusion protein accumulated at the PM specifically in a subapical region (Fig. 3D), which largely overlapped with the major domain of endocytic uptake of membrane lipids that was identified based on BFA treatment after FM4-64 labeling (Fig. 3, A, B, and C; Supplemental Fig. S11B). Figure 3D shows a representative image of an AtAP180::eYFP-expressing pollen tube. All analyzed pollen tubes continued to grow at a normal rate of at least 3 μm min^{-1} after confocal imaging, although they displayed a slight but statistically significant reduction in average growth rate as compared to control pollen tubes expressing free eYFP (Supplemental Fig. S13). The exact average length and position of the subapical PM domain at which AtAP180::eYFP accumulated is indicated in Figure 3C. As shown in this figure, the subapical PM domains identified based on AtAP180::eYFP imaging and on the analysis of loss of FM4-64 PM labeling after BFA treatment shared an identical length (~9 μm) and were largely overlapping. However, the AtAP180::eYFP-labeled domain was positioned 2.3 μm more distally (further away from the apex). AtAP180::eYFP was imaged in normally elongating pollen tubes, whereas analysis of loss of FM4-64 PM labeling was performed after BFA treatment, which effectively blocks pollen tube tip growth. This may be responsible for the 2.3-μm shift between the two domains, as PM domains at the pollen tube tip typically shift toward the apex upon inhibition of pollen tube growth (Helling et al., 2006; Zhao et al., 2010; Potocký et al., 2014). Unfortunately, this hypothesis could not be experimentally verified, as for unknown reasons AtAP180::eYFP did not detectably accumulate at the PM of pollen tubes treated with BFA to block FM4-64 recycling or with other drugs that inhibit pollen tube tip growth.

In any case, data resulting from confocal AtAP180::eYFP imaging provide compelling support for the presence of an about 9-μm-long major domain of endocytic uptake of lipid material within the subapical PM of tobacco pollen tubes, which was identified based on the analysis of loss of FM4-64 PM labeling after BFA treatment. Furthermore, the observed intracellular distribution of AtAP180::eYFP (1) indicates that in normally growing pollen tubes the proximal end of the identified subapical endocytic domain is positioned at a meridional distance of about 5.9 μm from the extreme apex and (2) strongly suggests that clathrin-mediated endocytosis occurs within this domain.

Unlike FM4-64-Labeled Lipid Material, TM Protein Markers for Membrane Traffic Are Not Subapically Endocytosed

Tobacco pollen tubes expressing NtINT4::eYFP, eYFP::AtRCI2a, or AtPRK1::eYFP were treated with BFA to test whether in the presence of this drug, similar to FM4-64 PM labeling (Fig. 3; Supplemental Fig. S11B, first row), PM labeling by these TM protein markers also massively decreases within the apical dome and the identified subapical endocytic domain 20 to 60 min after drug application. This would indicate that not only FM4-64-labeled lipid material but also TM marker proteins are endocytically internalized within this subapical domain. To our surprise, although a large number of pollen tubes expressing each of the three TM protein markers were observed by confocal time course imaging 0 to 180 min after BFA application, a reduction of PM-associated eYFP fluorescence within the apical dome or the subapical endocytic domain was never

observed (Fig. 4). In Figure 4A, representative images of different pollen tubes expressing each of the three TM marker proteins are presented, which were recorded by time course imaging during the indicated time periods after BFA application. Essentially stable labeling of the apical and subapical PM by each of the TM protein markers within the first 60 min after BFA application was also observed by time lapse imaging of individual pollen tubes (Supplemental Fig. S11B, rows 2–4). Quantitative analysis (Fig. 4B) of all NtINT4::eYFP- or eYFP::AtRCI2a-expressing pollen tubes investigated by time course imaging established that the relative intensity of PM labeling by these TM protein markers within the apical dome and the subapical endocytic region (normalized based on maximal intensity measured within both these two membrane domains in each analyzed pollen tube) remained close to 100% in the presence of BFA even after prolonged incubation. By contrast to NtINT4::eYFP and eYFP::AtRCI2a, AtPRK1::eYFP specifically accumulated to highest levels in the PM within the apical dome of untreated, normally growing tobacco pollen tubes (Fig. 1B).

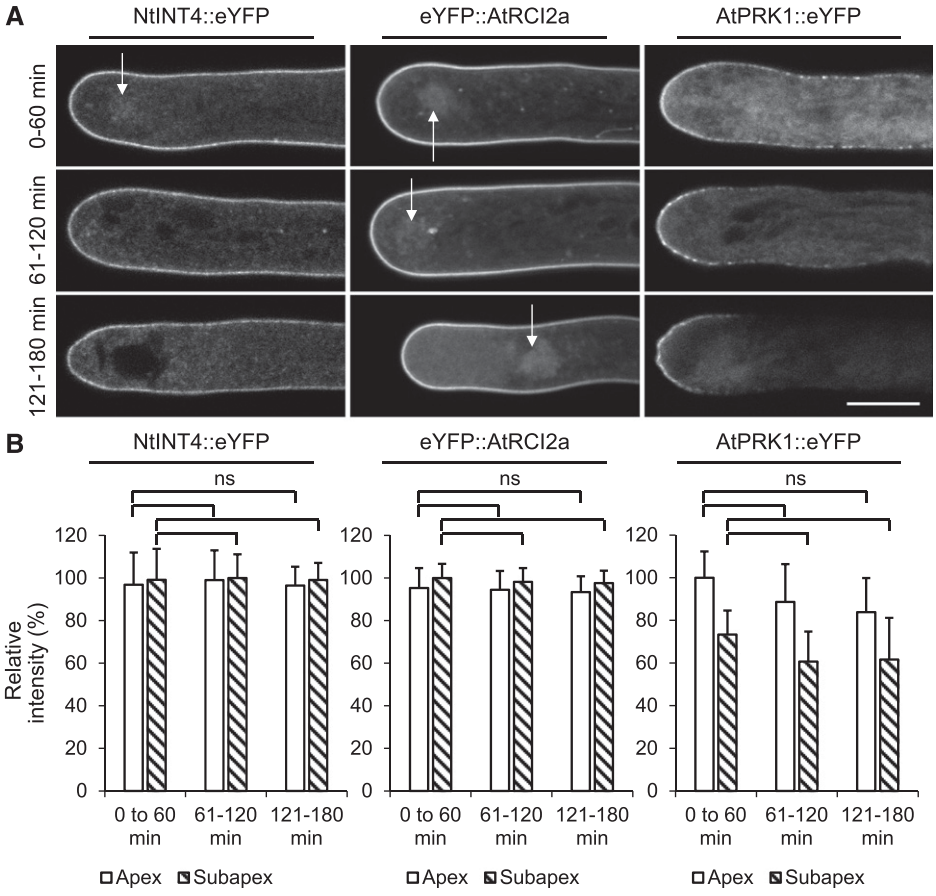

Figure 4. Time-course analysis of PM labeling by TM protein markers in tobacco pollen tubes after BFA application. A, Medial confocal optical sections through different representative pollen tubes transiently (AtPRK1::eYFP) or stably (NtINT4::eYFP; eYFP::AtRCI2a) expressing the indicated TM protein marker recorded after treatment with BFA (applied at 70 μM in 200 μL PTNT) for the indicated time period. Arrows, BFA compartment. Scale bar = 10 μm. As a result of the BFA treatment, tip growth of all analyzed pollen tubes was completely inhibited (Supplemental Fig. S8). During each time period after BFA application, all imaged pollen tubes expressing the same TM protein marker displayed highly similar PM labeling patterns (NtINT4::eYFP [three independent experiments], n = 78 [0–60 min], 61 [61–120 min], or 37 [121–180]; eYFP::AtRCI2a [five independent experiments], n = 85 [0–60 min], 82 [61–120 min], or 97 [121–180 min]; AtPRK1::eYFP [three independent experiments], n = 46 [0–60 min], 37 [61–120 min], or 31 [121–180 min]). B, Quantitative analysis of the average relative intensity of PM-associated TM protein marker fluorescence in all pollen tubes analyzed as described in A within the apical dome (Apex, meridional distance from the apex, 0–3.6 μm) and within the subapical endocytic region, which was identified based on BFA treatment of FM4-64-labeled pollen tubes as described in Figure 3 (Subapex, meridional distance from the apex, 3.6–12.6 μm). The intensity of PM-associated marker fluorescence was normalized in each analyzed pollen tube based on the maximal intensity measured with these two membrane domains (0–12.6 μm meridional distance from the apex), which was set to 100%. For each TM protein marker, the statistical significance of differences in the average intensity of PM-associated marker fluorescence during different time periods after BFA application was assessed separately within the apical dome and the subapical endocytic region using ANOVA (Dunnett's test, one-way). ns, Not significantly different ($P > 0.05$). Error bars = SD.

Consequently, the relative intensity of AtPRK1::eYFP PM labeling observed by time course imaging was lower within the subapical endocytic region than within the apical dome also in the presence of BFA (Fig. 4). However, the relative intensity of AtPRK1::eYFP PM labeling did not detectably change during BFA treatment in either of these two regions (Fig. 4B).

The PM distribution displayed by each of the analyzed TM protein makers during normal tip growth (Fig. 1) substantially changed after BFA-induced inhibition of this process (Fig. 4; Supplemental Fig. S11B). In the presence of this drug, NtINT4::eYFP and eYFP::AtRCI2a displayed an essentially even distribution within the PM, whereas AtPRK1::eYFP labeling of this structure increasingly assumed a dotted appearance and eventually completely disappeared in the shank. High turnover of this TM protein marker predominantly in the shank, which remained uncompensated because secretion was blocked, possibly contributed to this behavior. In any case, data shown in Figure 4 and in Supplemental Figure S11 demonstrate that by contrast to FM4-64-labeled lipid material, none of the analyzed TM protein markers was detectably internalized within the subapical endocytic PM region after BFA application.

Although in some pollen tubes imaged (as described in the previous paragraph) a typical subapical BFA compartment was visible after prolonged BFA incubation, invariably this compartment was only dimly labeled as compared to the PM (Fig. 4A; Supplemental Fig. S11B, arrows). Consistent with the persistence of TM protein marker labeling of the subapical endocytic PM domain in the presence of BFA (Fig. 4; Supplemental Fig. S11B), this observation suggests that TM protein markers are not endocytosed and cannot be delivered to the BFA compartment via this route. The weak labeling of the BFA compartment in some analyzed pollen tubes presumably is a consequence of redistribution of TM protein markers proteins already present within the secretory endomembrane system at the time of BFA application. As BFA blocks not only the formation of secretory vesicles at the TGN, but also ER to Golgi transport (Jiang and Rogers, 1998; Nebenführ et al., 2002), newly synthesized TM protein markers were unable to reach the BFA compartment in these experiments.

To confirm the data presented in Figure 4 and Supplemental Figure S11B, NtINT4::eYFP-, eYFP::AtRCI2a-, or AtPRK1::eYFP-expressing pollen tubes were colabeled for 30 min with FM4-64 and treated with BFA after the dye was washed out from the culture medium. Two-channel confocal time course imaging was employed to simultaneously observe the intracellular distribution of the TM protein markers (eYFP, green fluorescence) and of FM4-64 (red fluorescence) at different time points for 60 min after BFA application (Fig. 5). Consistent with observations described above (Fig. 3; Supplemental Fig. S11B), BFA induced a massive decrease of FM4-64 labeling of the PM early (21–40 min after application) within the subapical endocytic domain and later (41–60 min after application) also within the apical dome (Fig. 5, FM4-64). By contrast, no concomitant loss of PM labeling by any of the analyzed TM protein markers was detected in either of these two PM regions (Fig. 5, eYFP). Interestingly, a BFA compartment was occasionally visible in individual analyzed pollen tubes, which, relative to the PM, was labeled strongly by FM4-64 but only weakly by the expressed TM protein marker (Fig. 5, arrows). As discussed in the previous paragraph, this observation supports transport of FM4-64 but not of TM protein markers to the BFA compartment via endocytosis.

Together, data presented in Figures 4 and 5 and Supplemental Figure S11B establish that all analyzed TM protein markers are excluded from the massive internalization of FM4-64-labeled material observed within the subapical endocytic PM domain, which therefore appears to be specifically required for the recycling of excess lipid material delivered to the apical PM via secretion in tobacco pollen tubes.

The Subapical Endocytic PM Domain Partially Overlaps with a Detached TGN Compartment But Not with the F-actin Fringe

A subapically positioned VHAa1-positive (Dettmer et al., 2006) TGN compartment is postulated to act as a central sorting organelle with key functions in membrane traffic and in the recycling of PM material at the tip of growing tobacco pollen tubes (Stephan et al., 2014). This organelle is proposed to process membrane material delivered by endocytic vesicles to its distal surface and to recycle this material to secretory vesicles that are generated on its proximal surface (Stephan et al., 2014). Maintenance of the subapical position of this TGN compartment within the pollen tube cytoplasm depends on the F-actin fringe (Stephan et al., 2014), a cortical ring-like F-actin structure located close to the pollen tube apex (Kost et al., 1998; Chen et al., 2002; Lovy-Wheeler et al., 2005; Wilsen et al., 2006; Cheung et al., 2008; Vidali et al., 2009). An intact F-actin fringe appears to be essential for pollen tube tip growth (Bou Daher and Geitmann, 2011; Dong et al., 2012; Rounds et al., 2014; Stephan et al., 2014), possibly because of functions of this structure not only in TGN positioning but also directly in apical secretion (Cárdenas et al., 2008; Bou Daher and Geitmann, 2011; Dong et al., 2012; Rounds et al., 2014) and/or subapical endocytic membrane internalization (Samaj et al., 2006; Galletta and Cooper, 2009; Moscatelli et al., 2012; Meunier and Gutiérrez, 2016; Li et al., 2018).

To enhance our understanding of roles of the subapical TGN compartment and of the F-actin fringe in the endocytic uptake of FM4-64-labeled lipid material (Figs. 3 and 5; Supplemental Fig. S11B), the exact positions of these two structures in normally growing tobacco pollen tubes were mapped (Fig. 6) relative to each other and to the location of the subapical endocytic PM domain as determined based on AtAP180::eYFP

labeling (Fig. 3, C and D). The two F-actin markers eYFP::MTn (mouse talin; Kost et al., 1998) and lifeact::eYFP (Riedl et al., 2008; Vidali et al., 2009) both enable visualization of the F-actin fringe in tobacco pollen tubes displaying normal tip growth (Montes-Rodriguez and Kost, 2017). To noninvasively label the subapical VHAa1-positive TGN in such pollen tubes, eYFP fused to the ROP effector NtRISAP (eYFP::NtRISAP) can be employed (Stephan et al., 2014). Tobacco pollen tubes transiently expressing lifeact::eYFP, eYFP::MTn, or eYFP::NtRISAP at low levels under the control of the LAT52 promoter were imaged using confocal microscopy. Representative images of pollen tubes expressing each of these eYFP fusion proteins and growing essentially normally at a rate of at least 3 μm min^{-1} after confocal imaging (Supplemental Fig. S14) are shown in Figure 6A. Figure 6B presents the results of a quantitative and statistical analysis of the positions of the subapical TGN compartment and of the F-actin fringe in all imaged pollen tubes. The average meridional distance from the extreme apex (x = 0) of the most proximal and the most distal contact point of each of these two cytoplasmic structures with the PM is indicated in this figure. To facilitate direct comparison, the same figure also shows the position of the AtAP180::eYFP-labeled subapical endocytic PM domain in normally growing tobacco pollen tubes, which was determined as described above (Fig. 3, C and D). Together, data presented in Figure 6 allow the following interesting conclusions: (1) independently of the F-actin marker used, no overlap was observed between the F-actin fringe and the subapical endocytic PM domain, strongly suggesting that the F-actin fringe is not directly required for membrane internalization within this domain; (2) the F-actin fringe completely overlaps with the proximal half of the subapical TGN compartment, consistent with the reported essential function of the F-actin fringe in the cytoplasmic positioning of this compartment (Stephan et al., 2014); and (3) the distal half of the subapical TGN compartment overlaps with a short (~1.5 μm) subdomain

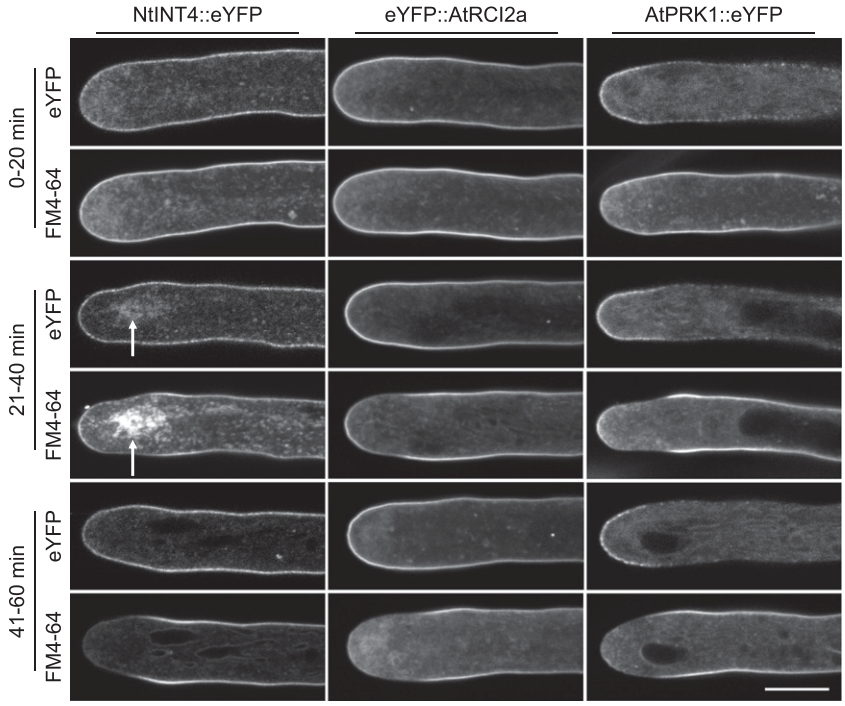

Figure 5. Simultaneous time course analysis of FM4-64 and TM protein marker PM labeling in BFA-treated tobacco pollen tubes. Medial confocal optical sections through different representative pollen tubes transiently (AtPRK1::eYFP) or stably (NtINT4::eYFP, eYFP::AtRCI2a) expressing the indicated TM protein marker, which had been grown in the presence of FM4-64 (applied at 50 μM in 200 μL PTNT) for 30 min before the dye was washed out from the culture medium and BFA was applied for the indicated time period (70 μM in 200 μL PTNT). eYFP fusion proteins serving as TM protein markers (green fluorescence, eYFP) and FM4-64 (red fluorescence, FM4-64) were simultaneously imaged in separate channels. As a result of the BFA treatment, tip growth of all analyzed pollen tubes was completely inhibited (Supplemental Fig. S8). During each of the indicated time periods, all imaged pollen tubes displayed essentially the same patterns of FM4-64 and of TM marker protein specific eYFP labeling of the PM (NtINT4::eYFP [two independent experiments], n = 11 [0–20 min], 22 [21–40 min], or 19 [41–60 min]; eYFP::AtRCI2a [two independent experiments], n = 10 [0–20 min], 22 [21–40 min], or 22 [41–60 min]; AtPRK1::eYFP [four independent experiments], n = 10 [0–20 min], 16 [21–40 min], or 23 [41–60 min]). The BFA compartment visible in the NtINT4::eYFP-expressing pollen tube shown (21–40 min after BFA application) was clearly more strongly labeled by FM4-64 than by NtINT4::eYFP (ratio between the average fluorescence intensities displayed by the BFA compartment and by the apical PM, 1.39 [FM4-64] and 0.65 [NtINT4::eYFP]). Arrow, BFA compartment. Scale bar = 10 μm.

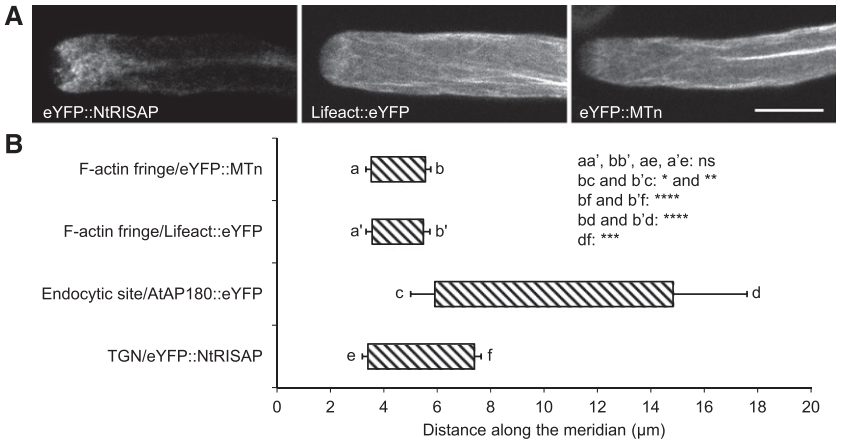

Figure 6. Positional mapping of a detached TGN compartment and of the F-actin fringe relative to each other and to the subapical endocytic PM domain in tobacco pollen tubes. A, Medial confocal optical sections through representative essentially normally growing pollen tubes transiently expressing the TGN marker eYFP::NtRISAP ($n = 13$, four independent experiments) or one of the F-actin markers Lifeact::eYFP ($n = 17$, three independent experiments) or eYFP::MTn ($n = 19$, three independent experiments). All pollen tubes expressing the same marker displayed highly similar eYFP labeling patterns. Growth rate of the pollen tubes shown (after confocal imaging), 3.6 μm min^{-1} (eYFP::NtRISAP), 5.4 μm min^{-1} (Lifeact::eYFP), and 4.8 μm min^{-1} (eYFP::MTn). Scale bar, = 10 μm. B, Quantitative analysis of the meridional distance from the extreme apex ($x = 0$ μm) of the most proximal and the most distal contact points of the NtRISAP-associated TGN compartment or of the F-actin fringe, with the PM in all pollen tubes analyzed as described in A. For direct comparison, the position of the AtAP180::eYFP-labeled subapical endocytic PM domain, which was determined in normally growing pollen tubes as described above (Fig. 3, C and D), is also indicated. Exact extensions of domains shown are as follows: 3.4 ± 0.21 to 7.4 ± 0.26 μm (TGN; eYFP::NtRISAP), 3.6 ± 0.23 to 5.5 ± 0.25 μm (F-actin fringe; lifeact::eYFP), 3.5 ± 0.20 to 5.6 ± 0.20 μm (F-actin fringe; eYFP::MTn), and 5.9 ± 0.91 to 14.8 ± 2.8 μm (subapical endocytic domain; AtAP180::eYFP). The statistical significance of differences between the average meridional distances of proximal and distal ends (a, a', b, b', c, d, e, and f) of different PM domains were analyzed as indicated using ANOVA (Tukey's test, one-way). Note that the distal end of the F-actin fringe (irrespective of the marker used) and the proximal end of the subapical endocytic domain are statistically significantly different (bc, b'c). *$P \leq 0.05$; **$P \leq 0.01$; ***$P \leq 0.001$; and ****$P \leq 0.0001$; ns, not significantly different ($P > 0.05$). Error bars = SD.

at the proximal end of the subapical endocytic PM region, a spatial arrangement that is fully consistent with the proposed delivery of internalized membrane material by endocytic vesicles to the distal surface of this compartment.

BFA treatment not only blocks secretion but also rapidly disrupts the subapical F-actin fringe at the pollen tube tip (Rounds et al., 2014). To further investigate a possible role of the F-actin fringe in membrane internalization within the subapical endocytic PM region, pollen tubes transiently expressing eYFP::MTn or lifeact::eYFP were colabeled for 30 min with FM4-64 before the dye was washed out from the culture medium and BFA was applied. Two-channel confocal time course imaging was performed to simultaneously visualize F-actin organization (eYFP; green fluorescence) and FM4-64 labeling (red fluorescence) at different time points during the first 60 min after BFA application (Fig. 7). BFA treatment (1) stopped pollen tube growth (Supplemental Fig. S8), (2) rapidly (0–20 min after drug application) disrupted the subapical F-actin fringe (Fig. 7, eYFP), and (3) as previously demonstrated (Figs. 3 and 5; Supplemental Fig. S11B, first row), induced a massive decrease of FM4-64 labeling of the PM first (21–40 min after drug application) within the subapical endocytic domain and later (41–60 min after drug application) also within the apical dome (Fig. 7, FM4-64). The same observations were also made by time lapse imaging of lifeact::eYFP-expressing and FM4-64-labeled individual pollen tubes after the application of BFA either alone or in combination with the actin disrupting drug Latrunculin B (LatB; Supplemental Fig. S15). Combined application of BFA and LatB not only caused rapid disruption of the F-actin fringe but also strongly affected longitudinally oriented F-actin fibers. Together, these findings demonstrate that internalization of FM4-64-labeled lipid material within the subapical endocytic PM domain can occur in the absence of an intact F-actin fringe.

Data presented in this section firmly establish that, consistent with the observed lack of overlap between the F-actin fringe and the subapical endocytic PM domain (Fig. 6), drug-induced F-actin fringe disruption does not affect the internalization of lipid material within this membrane domain (Fig. 7). The F-actin fringe therefore clearly has no direct function in this process. However, previously reported (Stephan et al., 2014) key functions of the F-actin fringe in the positioning of a subapical TGN compartment, as well as of this TGN compartment in the recycling of endocytosed PM material, are supported by the quantitative structural data shown in Figure 6. Consequently, the F-actin

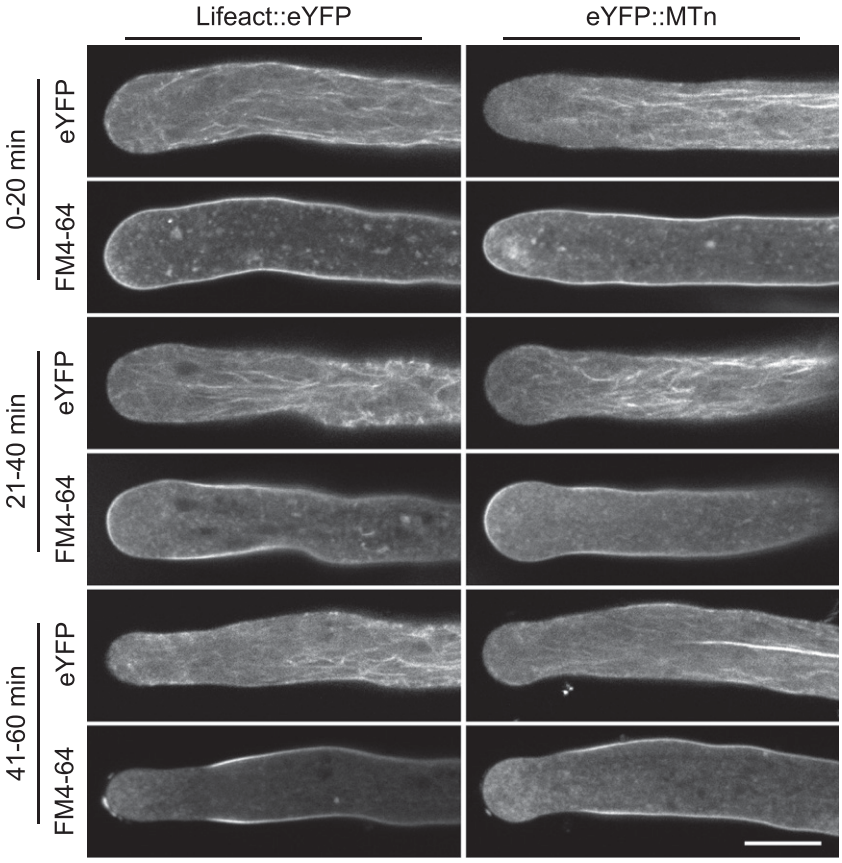

Figure 7. Simultaneous time course analysis of FM4-64 PM labeling and of noninvasively visualized F-actin structures in BFA-treated tobacco pollen tubes. Medial confocal optical sections through different representative pollen tubes transiently expressing the indicated noninvasive F-actin markers (Lifeact::eYFP or eYFP::MTn), which had been grown in the presence of FM4-64 (applied at 50 μM in 200 μL PTNT) for 30 min before the dye was washed out from the culture medium and BFA was applied for the indicated time period (70 μM in 200 μL PTNT). Lifeact::eYFP or eYFP::MTn fusion proteins (green fluorescence, eYFP) and FM4-64 (red fluorescence, FM4-64) were simultaneously imaged in separate channels. As a result of the BFA treatment, tip growth of all analyzed pollen tubes was completely inhibited (Supplemental Fig. S8). During each of the indicated time periods, all imaged pollen tubes displayed essentially the same FM4-64 PM labeling patterns (FM4-64) and very similar F-actin structures (eYFP) labeled by one of the two noninvasive markers (Lifeact::eYFP [three independent experiments], $n = 13$ [0–20 min], 14 [21–40 min], or 13 [41–60 min]; eYFP::MTn [four independent experiments], $n = 16$ [0–20 min], 24 [21–40 min], or 14 [41–60 min]). Scale bar = 10 μm.

fringe may be essential for pollen tube tip growth because it is required for apical membrane recycling based on its function in maintaining the positioning of the subapical TGN compartment.

Mathematical Modeling of Steady-State Marker Distribution within the PM

To enhance our understanding of the distinct steady-state distribution patterns within the pollen tube PM, which are displayed by different markers for membrane traffic (Fig. 1, B and C), these distribution patterns were mathematically modeled based on a number of assumptions, which are discussed below and are largely derived from experimental data reported here. Some of these assumptions may be considered modeling output, as they have emerged from the process of fitting the model to experimental data.

The model divides the PM into the following four regions, which are positioned at the indicated meridional distances from the extreme apex: apical dome (0–3.5 μm), F-actin fringe region (3.5–5.5 μm), subapical region (5.5–15 μm), and shank (>15 μm). The positioning of these regions emerged from model fitting and is in close agreement with experimental data (Fig. 6). Four processes are modeled, which together determine marker dynamics and steady-state distribution within the PM. The extreme pollen tube apex is defined as a reference point with a fixed position. Consequently, all markers of membrane traffic within each of the four PM regions are subject to a constant retrograde flux at the rate of pollen tube tip growth (process 1), which has been experimentally determined as discussed above (Supplemental Fig. S1). The density of individual markers can locally increase (source) or decrease (sink) within the PM as a result of cytoplasmic vesicle traffic (process 2). A source may result either from secretion or from local increase in TM protein marker density caused by selective endocytosis of lipid material. By contrast, a sink corresponds to endocytic internalization. In addition, diffusion within the PM (process 3) is expected to occur with marker- and region-specific coefficients. Finally, fitting to experimental plots of marker distribution within the PM in the shank required the model to account for marker degradation, which in the case of FM4-64 is overcompensated by ongoing PM staining by residual dye present in culture medium (process 4).

To compute distribution profiles of all analyzed markers within the PM, model equations were adjusted to account for different sets of the four processes introduced in the previous paragraph occurring in each of the four different regions of the pollen tube PM (Table 1). The F-actin fringe region, in which, apart from retrograde flux, only diffusion is assumed to occur, is modeled such that it links the solutions of the equations describing marker distribution within the apical and

Table 1. *Processes assumed by the model to substantially contribute to marker distribution profiles within the indicated regions of the pollen tube PM (marked by "+")*

Region	Retrograde Flux	Source/Sink	Diffusion	Marker Protein Degradation (*K*) Staining by Residual FM4-64 (*R*)	
	(v_0)	(Q, q)	(D)	(K)	(R)
Apical (*a*)	+	+	+	—	—
F-actin fringe	+	—	+	—	—
Subapical (*sa*)	+	+	+	+	—
Shank (*s*)	+	—	+	+	+

the subapical regions. Hence, within the F-actin fringe region, the diffusion coefficient of each marker undergoes transition between the apical and subapical values. No source or sink is assumed to be present in the shank region. Furthermore, the diffusion coefficients of all markers in the subapical region and in the shank are assumed equal. Marker degradation is also defined to occur at equal rates in the subapical region and in the shank but has been assigned the value zero in the apical region, in which degradation presumably is irrelevant compared to changes in marker density resulting from vesicle traffic. In addition, the model implicates that ongoing PM staining by residual FM4-64 is overcompensating degradation of this lipid dye in all PM regions and substantially contributes to its distribution profile only in the shank. The rates or coefficients of all processes other than retrograde flux (Q, source; q, sink; D, diffusion; K, marker protein degradation; R, staining by residual FM4-64) are variables that can be read out after model fitting (Table 2).

To fit the model to experimental line plots displaying average intensity of PM-associated marker fluorescence (Fig. 1, B and C), these line plots needed to be normalized based on the values at the extreme apex, which were set to the intensity level "1" (Fig. 8, light blue line). Consequently, the Q, q, D, K, and R values read out for the different markers after model fitting (Table 2) are based on relative levels of PM-associated marker fluorescence but not on absolute marker density. For all analyzed markers, an excellent fit of the model (Fig. 8, brown line) to the experimental data were obtained, after the following marker-specific adjustments were made: (1) Because fitting the model to the AtPRK1::eYFP line plot indicated a much stronger source of this marker within the apical dome (Q_a) than in the subapical region (Q_{sa}), Q_{sa} could not be accurately determined and was defined to be zero ($Q_{sa} = 0$) for practical purposes. Hence, for AtPRK1::eYFP, only Q_a and D_a within the apical dome could be read out as independent values after model fitting (Table 2). (2) Furthermore, as the experimental NtINT4::eYFP distribution plot displays a distinct kink at the border between the apical dome and the F-actin fringe region (Figs. 1B and 8), the requirement for smoothness in the marker distributions at this border was removed from the model. (3) Finally, selective endocytosis of lipid material within the subapical endocytic domain locally increases TM protein marker density with a rate that is independent of this density, whereas the rate of FM4-64 internalization resulting from the same process obviously increases with higher dye concentrations within the PM. To model FM4-64 distribution within the subapical PM, the term $q_{sa}c(x,t)$ was therefore employed instead of the constant Q_{sa} that was used for TM protein modeling. By contrast, TM protein degradation occurs at a concentration-dependent rate, whereas the rate of ongoing PM staining by residual FM4-64 present in the culture medium is not affected by the dye concentration within the PM. Therefore, the term $K_s\, c(x,t)$ (equal to $K_{sa}\, c(x,t)$) was used to describe TM protein degradation, whereas the concentration-independent constant R_s was employed to represent membrane labeling by residual FM4-64.

The possibility to obtain an excellent fit of the model to the experimental data (Fig. 8), along with the signs of the Q_a, Q_{sa}, and q_{sa} values read out for all analyzed markers (Table 2), are consistent with and further support the following key experimental findings: (1) all markers of membrane traffic are incorporated into the PM as a consequence of secretion occurring within the apical dome (positive Q_a values), and (2) FM4-64-labeled PM material is endocytically recycled within the subapical region (negative q_{sa} value), whereas TM protein markers are not (positive Q_{sa} values). Furthermore, interactions of the extracellular LRR domain of AtPRK1 with the cell wall, which were proposed to contribute to the experimentally detected accumulation of this protein to highest levels within the apical dome (Fig. 1B), are supported by the observation that AtPRK1 displays the lowest D_a value ($0.040 \pm 0.003\ \mu m^2\ s^{-1}$) of all TM protein markers tested, including a truncated form of this protein missing the extra cellular LRR domain ($0.063 \pm 0.003\ \mu m^2\ s^{-1}$; Table 2).

In addition, model output summarized in Table 2 allows a number of further interesting conclusions, which remain to be experimentally verified. It is not possible to directly compare absolute Q_a, Q_{sa}, or q_{sa} values between markers, as experimental line plots were normalized for model fitting and because the correlation between marker fluorescence and density within the PM has not been quantified. Distinct Q_{sa} values were therefore read out for different TM protein

Table 2. *Readout after model fitting to experimental data*

TMP, Transmembrane proteins. n.a., Not available.

Region	Parameter	Unit	NtINT4	AtRCI2a	AtPRK1	AtPRK1 ΔSP-LRR	FM4-64
Apical	Q_a	$\mu m^{-1}\ s^{-1}$	6.0 ± 0.3	2.6 ± 0.2	8.3 ± 0.6	6.3 ± 0.3	10.0 ± 0.5
	D_a	$\mu m^2\ s^{-1}$	0.085 ± 0.004	0.051 ± 0.003	0.040 ± 0.003	0.063 ± 0.003	0.034 ± 0.002
Subapical	Q_{sa} (TMP)[a]	$\mu m^{-2}\ s^{-1}$	0.31 ± 0.02	5.7 ± 0.4	n.a.	1 ± 0.2	–
	q_{sa} (FM4-64)[b]	s^{-1}	–	–	–	–	− (0.21 ± 0.01)
	D_{sa}[c]	$\mu m^2\ s^{-1}$	0.37 ± 0.05	0.79 ± 0.05	n.a.	0.45 ± 0.05	1.21 ± 0.06
Ratio values	Q_a/Q_{sa} (TMP)	μm	19.3548	0.4561	n.a.	6.3	–
	Q_a/q_{sa} (FM4-64)	μm^{-1}	–	–	–	–	−47.6190
Shank	K_s[d] (TMP)[b]	$10^{-2}\ s^{-1}$	-(0.72 ± 0.04)	-(0.83 ± 0.05)	n.a.	-(0.36 ± 0.06)	–
	R_s (FM4-64)[a]	$\mu m^{-2}\ s^{-1}$	–	–	–	–	0.40 ± 0.02

[a]Concentration independent. [b]Concentration dependent. [c]$D_{sa} = D_s$. [d]$K_s = K_{sa}$.

markers, although local enrichment of all these markers resulting from selective endocytosis of lipid material within the subapical region is expected to occur at the same rate. However, the Q_a/Q_{sa} or Q_a/q_{sa} ratio, as well as D, K, and R values are not affected by data normalization and can be directly compared between markers. The particularly low Q_a/Q_{sa} ratio obtained for eYFP::AtRCI2a (0.4561 μm; Table 2) indicates that this protein is apically secreted at a low rate as compared to the rate of the accumulation of this protein within the subapical region, which is caused by selective endocytosis of lipid material. Together with relatively fast degradation in the shank ($K_s = -0.83 \pm 0.05\ 10^{-2}s^{-1}$; Table 2), this may explain the massive eYFP::AtRCI2a accumulation that is experimentally observed within the lateral PM. Furthermore, as discussed above, model

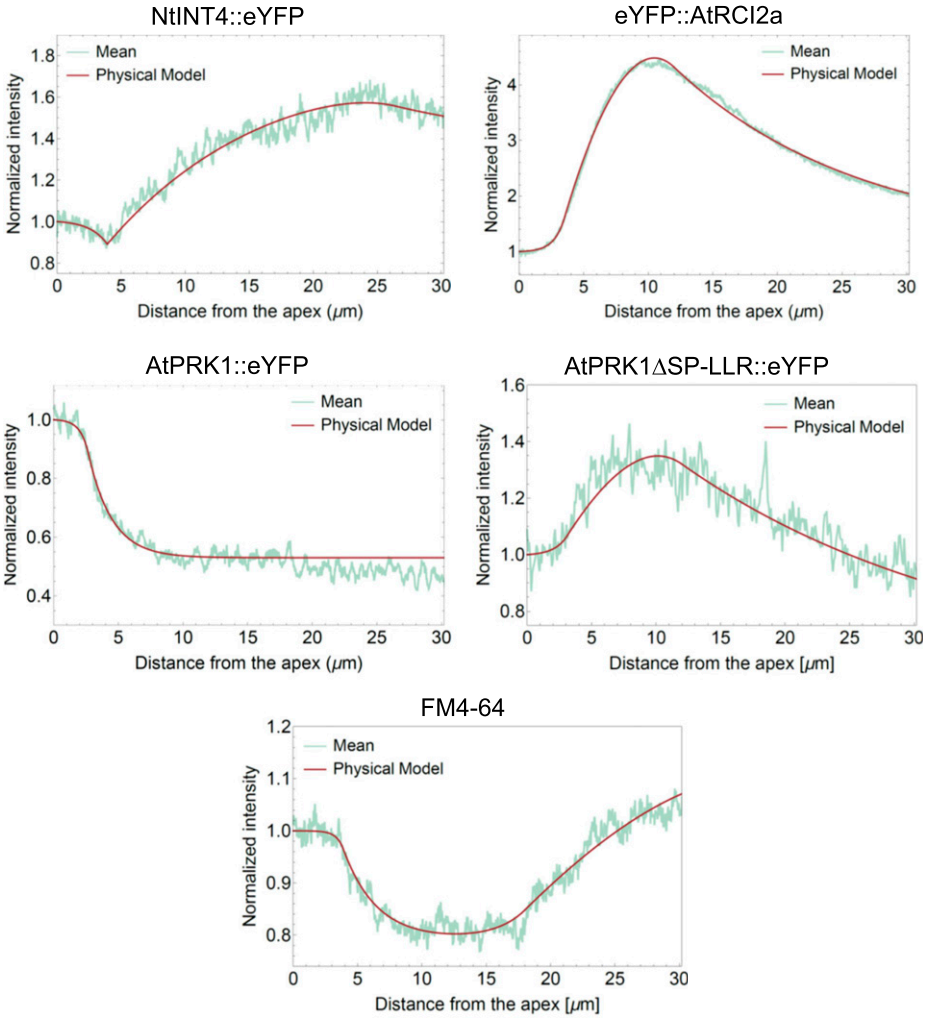

Figure 8. Fitting of a mathematical model of steady-state marker distributions within the pollen tube PM to experimental data. The experimental line plots depicted in light blue represent the steady-state distribution of the indicated markers for membrane traffic within the PM and show the average intensity of PM-associated marker fluorescence at different meridional distances from the extreme pollen tube apex. The same line plots are also presented in Figure 1, B and C, but are displayed here after normalization based on the values at the extreme apex ($x = 1$). The brown lines represent output of a mathematical model of steady-state marker distribution described in detail in the text, after model fitting to the experimental line plots. The excellent fit obtained for all markers strongly supports model relevance. Table 2 summarizes model readout obtained after fitting, which provides information concerning the rate and spatial organization of cellular processes (including secretion, endocytosis, diffusion, and degeneration), which determine marker dynamics and steady-state distribution.

fitting required that all TM marker proteins are degraded at a low rate in both the subapical and shank regions and that constant relabeling of the PM by residual FM4-64 in the culture medium compensates degradation of this dye, a process that substantially contributes to the FM4-64 distribution profile specifically in the shank. Finally and most interestingly, whereas within the subapical and shank regions of the PM the diffusion coefficients (Table 2) of all TM proteins markers (D_{sa} = 0.37–0.79 $\mu m^2\ s^{-1}$) and of FM4-64 (D_{sa} = 1.21 $\mu m^2\ s^{-1}$) are within the typical range for TM proteins (Edidin, 1987; Vrljic et al., 2002; Hartel et al., 2015) and membrane lipids (Edidin, 1987), respectively, diffusion of all markers appears to be strikingly slow within the apical dome (0.034 to 0.085 $\mu m^2\ s^{-1}$; Table 2). This observation may be a consequence of substantial molecular crowding, possibly resulting from the massive secretory activity within this PM region, and certainly warrants experimental confirmation.

DISCUSSION

Quantitative Structural Organization of Apical Membrane Traffic at the Pollen Tube Tip

Our results are essentially consistent with the classical model of apical membrane traffic at the tip of elongating pollen tubes. This model predicts that bulk secretion required for cell wall biogenesis, as well as for the coordination of signaling processes controlling tip growth (Luo et al., 2017; Li et al., 2018), occurs apically and results in the deposition of excess material in the PM, which is recycled based on massive subapical endocytosis (Fig. 9). Evidence presented here shows that in growing tobacco pollen tubes, newly synthesized TM protein markers and endocytically recycled FM4-64-labeled membrane lipids are specifically delivered by secretion to the PM within a small domain at the tip, which extends from the extreme apex to the subapical F-actin fringe (meridional distance from the extreme apex, 0 to ~3.5 μm). Furthermore, we demonstrate that bulk endocytic internalization of FM4-64-labeled membrane material, from which all analyzed TM protein markers are excluded, occurs within a subapical PM domain located distal to the F-actin fringe (meridional distance from the extreme apex in normally growing pollen tubes, 5.9–14.8 μm).

In addition, data described here further support a previously suggested (Stephan et al., 2014) important function of a subapical TGN compartment as a central sorting organelle in tobacco pollen tubes, with which Golgi-derived and endocytic vesicles delivering newly synthesized or recycled membrane material, respectively, may fuse at the distal end, and which may generate secretory vesicles at its proximal surface (Fig. 9). In addition to the typical trans-Golgi-associated TGN, separate detached TGN elements are frequently observed in plant cells (Zárský et al., 2009; Uemura, 2016; Uemura et al., 2019), which in tobacco pollen tubes appear to aggregate to a single subapical compartment. Presumably, a key function of this TGN compartment is to maintain the massive accumulation of secretory vesicles within the cytoplasmic ARVA at the pollen tube tip, for which no plausible alternative mechanism has been proposed to date. Maintenance of the positioning of the subapical TGN compartment within a pollen tube region displaying rapid cytoplasmic streaming requires an intact F-actin fringe (Stephan et al., 2014). Results of the exact positional mapping of the endocytic PM domain, the F-actin fringe, and the TGN compartment to distinct subapical regions of tobacco pollen tubes, which are presented here, are fully consistent with the proposed functions of the subapical TGN compartment in membrane traffic, as well as of the F-actin fringe in the subapical cytoplasmic positioning of this compartment. The proximal end of the subapical TGN compartment precisely colocalizes with the F-actin fringe, whereas the distal end of this compartment overlaps with a small proximal region

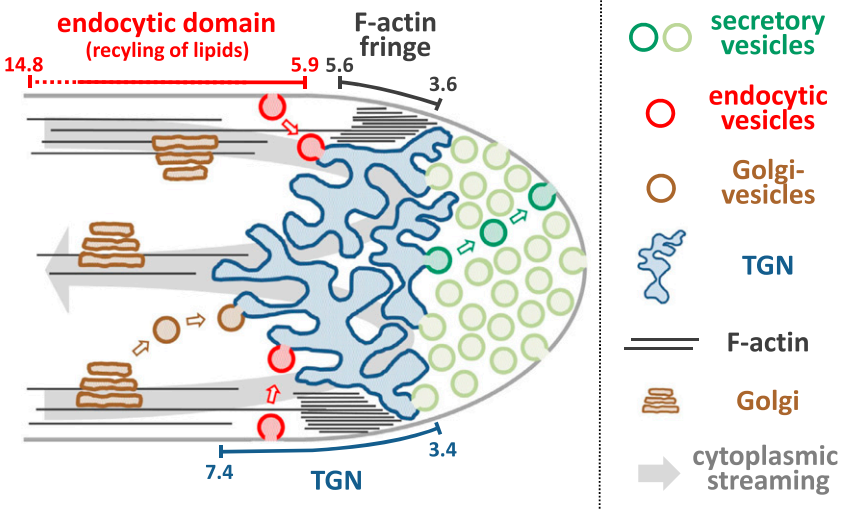

Figure 9. Model of apical membrane traffic underlying tobacco pollen tube tip growth. Secretion required for cell wall biogenesis occurs within the apical dome (0–3.5 μm meridional distance from the extreme apex) and results in the incorporation of excess lipid material into the PM, which is recycled by subapical endocytosis (5.9–14.8 μm meridional distance from the extreme apex). A subapical TGN compartment (PM contacts, 3.4–7.4 μm meridional distance from the extreme apex) serves as a central sorting organelle with which Golgi-derived as well as endocytic vesicles fuse at the distal end and which generates secretory vesicles at its proximal surface. The cortical F-actin fringe (3.6–5.6 μm meridional distance from the extreme apex) maintains the positioning of the subapical TGN compartment within a pollen tube region displaying rapid cytoplasmic streaming.

(~1.5 μm long) of the subapical endocytic domain (Figs. 6 and 9).

Interestingly, our results demonstrate that the F-actin fringe does not overlap at all with the subapical endocytic domain and is not required for the internalization of FM4-64-labeled membrane lipids within this domain. Furthermore, the structural organization at the tip of tobacco pollen tubes, which emerges from data presented here, does not suggest a direct function of the F-actin fringe in the transport of secretory vesicles to sites of fusion with the PM (Fig. 9). An intact F-actin fringe may therefore be essential for pollen tube tip growth (Bou Daher and Geitmann 2011; Dong et al., 2012; Rounds et al., 2014) exclusively because it is required for the maintenance of the cytoplasmic positioning of the subapical TGN compartment. Fine F-actin filaments have been observed within the cytoplasmic ARVA at the pollen tube tip in some studies (Lancelle and Hepler, 1992; Miller et al., 1996; Fu et al., 2001; Qu et al., 2013) and are proposed to serve as tracks for the myosin-mediated transport of secretory vesicles toward the PM (Fu and Yang, 2001; Kost, 2008; Qu et al., 2013; Stephan et al., 2014). However, it is debatable whether such filaments can be unequivocally detected using available in vivo markers in normally growing pollen tubes of tobacco and other plant species (Fig. 6A; Kost et al., 1998; Montes-Rodriguez and Kost, 2017; Qu et al., 2017). In these pollen tubes, the constant supply of secretory vesicles budding from the proximal surface of the subapical TGN compartment may be sufficient to push these vesicles forward toward sites of fusion with the apical PM (Fig. 9).

Identification of Major Sites of Secretion and Endocytosis

To identify sites of bulk secretion and endocytosis in tobacco pollen tubes, different in vivo markers for membrane traffic with highly diverse characteristics were employed in this study: the fluorescent lipid dye FM4-64 as well as three TM proteins with distinct sizes, numbers of TM domains, functions, and origins, which all carried an eYFP tag attached to a cytoplasmic terminus. Although in the case of eYFP::AtRCI2a different topology prediction tools (e.g. SPOCTOPUS [Viklund et al., 2008] and Phobius [Käll et al., 2007]) indicate extracellular localization of both termini, these predictions appear to be wrong (Thompson and Wolniak, 2008). The use of four highly diverse membrane transport markers enabled the discovery of basic principles of protein and lipid trafficking underlying tobacco pollen tube tip growth irrespective of marker-specific targeting mechanism, which may include interaction with unequally distributed cell wall components. The steady-state distribution patterns of three analyzed markers (FM4-64, NtINT4::eYFP, eYFP::AtRCI2a) did not show PM accumulation preferentially within the apical dome. However, consistent with bulk secretion occurring apically, the PM within the apical dome of pollen tubes expressing each of these markers displayed similar levels of steady-state labeling as apical secretory vesicles accumulating in the underlying cytoplasm (Fig. 1, B and C). Only the TM protein marker AtPRK1::eYFP showed steady-state accumulation at clearly higher levels within the apical PM as compared to other PM regions as well as to apical secretory vesicles. Interestingly, interactions of the extracellular LRR domain of AtPRK1 with the apical cell wall appear to be primarily responsible for this distribution pattern, as strongly suggested by the observations that truncated AtPRK1::eYFP missing the LRR domain fails to specifically accumulate within the apical PM (Fig. 1B) and appears to display faster diffusion within this membrane region than full-length AtPRK1::eYFP (Table 2). Additional imaging and modeling results strongly suggest that not only marker-specific interactions with cell wall components, but also distinct rates of apical secretion, subapical endocytosis, and degradation, are responsible for the observed striking differences in the steady-state distribution patterns of some of the analyzed markers. Together, these findings demonstrate that steady-state distribution patterns of markers for membrane traffic do not directly indicate the location of sites of bulk secretion or endocytosis in pollen tubes.

The site of bulk secretion in tobacco pollen tubes was identified based on two completely different approaches, which enabled investigation of the dynamic behavior of markers for membrane traffic during normal tip growth: (1) analysis of the recovery of TM protein marker fluorescence after photobleaching pollen tube tips and (2) imaging FM4-64 redistribution after the initial even PM labeling by this dye. The results of the application of these two approaches demonstrated that both newly synthesized TM protein markers as well as endocytically recycled FM4-64-labeled membrane lipids are incorporated into the PM specifically within the same central region of the apical dome (Fig. 9). Furthermore, the site of bulk endocytic membrane internalization in tobacco pollen tubes was also identified using two entirely different approaches: (1) analysis of loss of marker labeling of the PM after BFA treatment, which blocks secretion without preventing endocytosis and (2) in vivo imaging of the PM association of AtAP180::eYFP, a marker for clathrin-mediated endocytosis at the PM. FM4-64-labeled membrane lipids, but none of the analyzed TM protein markers, were internalized, apparently by clathrin-mediated endocytosis within a clearly defined subapical PM domain (Fig. 9). Consistent with this conclusion, marker distribution profiles presented in Figure 1 show that levels of PM-associated marker fluorescence are substantially reduced within the subapical endocytic domain in FM4-64-labeled pollen tubes both at the redistribution and the steady-state stage, whereas this is clearly not the case in pollen tubes expressing NtINT4::eYFP and AtPRK1ΔSP-LRR::eYFP, which otherwise display similar steady-state distribution patterns as FM4-64. Subapical clathrin-mediated endocytosis during tip growth is strongly supported also by previously

published reports showing that not only fluorescent AtAP180 fusion proteins (Zhao et al., 2010; Kaneda et al., 2019), but also other markers for clathrin-mediated endocytosis, including AtDRP1C::RFP (ARABIDOPSIS DYNAMIN-RELATED PROTEIN1C; Sekeres et al., 2017), PICALM5a::GFP, PICALM5b::GFP, EAP::RFP (AtAP180-related ANTH domain-containing containing proteins), and CLC1::GFP (CLATHRIN LIGHT CHAIN1; Muro et al., 2018; Li et al., 2018), specifically accumulate at the subapical PM in elongating tobacco and/or Arabidopsis pollen tubes.

Internalization of Membrane Lipids and, Possibly, Selected Proteins by Subapical Endocytosis

As discussed above, FM4-64-labeled structural lipid components of the membrane of secretory vesicles appear to be incorporated in excess amounts into the PM as a consequence of apical secretion required for cell wall biogenesis and therefore need to be constitutively recycled by subapical endocytic internalization, which was observed not only in BFA-treated tobacco pollen tubes (Figs. 3, 5, and 7; Supplemental Figs. S11B, S12, and S15), but also during normal tip growth (Fig. 1). Perhaps it is not surprising that by contrast to FM4-64-labeled lipids, none of the analyzed TM protein markers were internalized within the subapical endocytic PM domain. Many TM proteins presumably have functions all along the pollen tube cell and are delivered by apical secretion to the PM at a rate determined by expression level, which ensures maintenance of adequate protein activity as required for tip growth. Subapical endocytic recycling of such proteins would not serve any apparent purpose, although these proteins of course are expected to be turned over just like every other cellular factor. In fact, fitting mathematically modeled intracellular distributions of analyzed TM protein makers to experimental data required the assumption that these markers are degraded within the pollen tube shank (Table 2).

However, endocytic recycling plays a key role in polarizing the accumulation of some TM proteins within specific PM domains in different types of plant cells (e.g. PIN auxin efflux carriers; Geldner et al., 2003; Paciorek et al., 2005). Although our data show that apical AtPRK1 accumulation in tobacco pollen tubes does not depend on subapical endocytosis but requires interactions with the apical cell wall, observations reported in the literature strongly suggest that subapical endocytic internalization is essential for the preferential accumulation of other proteins at the pollen tube apex. The PME inhibitor AtPMEI2, a secreted soluble protein that specifically accumulates within the apical cell wall of tobacco pollen tubes, was detected in BFA compartments in these cells, indicating that this protein is subapically endocytosed (Röckel et al., 2008). Furthermore, the specific accumulation of the RLK ANXUR, which contains a single TM domain, within the PM at the apex of Arabidopsis pollen tubes requires subapical clathrin-mediated endocytic uptake, which depends on the AtAP180-related ANTH domain-containing proteins PICALM5a and PICALM5b (Muro et al., 2018). Interestingly, the study by these authors showed that by contrast to ANXUR, the apical accumulation of another RLK with a single TM domain (AtPRK6) was not affected in *picalm5* mutants, confirming that apical accumulation of TM proteins in pollen tubes can depend on different mechanisms. In any case, subapical endocytic internalization responsible for apical polarization of pollen tube TM or cell wall proteins is expected to depend on specific signals, which appear to be absent from all TM protein markers analyzed in the study presented here. In fact, specific interaction with the WD40 protein At-REN4 was recently proposed to induce subapical clathrin-mediated endocytic internalization of active At-ROP1, which appears to contribute to the maintenance of the specific accumulation of this protein at the pollen tube apex (Li et al., 2018). At-ROP1 is a prenylated peripheral membrane protein, which belongs to the ROP GTPase family and plays a key role in the control of tip growth (Qin and Yang, 2011).

Drift and Diffusion of PM Components

Membrane traffic at the pollen tube tip (Fig. 9) is proposed to result in constant retrograde drift of PM material from the apical site of secretion to the subapical endocytic domain (Kost, 2008; Grebnev et al., 2017). Consistent with this hypothesis, in BFA-treated tobacco pollen tubes, FM4-64-labeled membrane lipids appear to drift or diffuse from the apical dome to the lateral endocytic domain, where they are endocytosed (Figs. 3, 5, and 7; Supplemental Figs. S11B, S12, and S15). Furthermore, after photoconversion at the apex of Arabidopsis pollen tubes, red fluorescent AtPRK1::Dendra2 also appears to move within the PM from the apical dome to lateral regions (Luo et al., 2016). Interestingly, results of mathematical modeling of TM protein marker and FM4-64 distributions, which are presented here, indicate that both TM proteins and membrane lipids display typical diffusion coefficients within the PM in all regions of tobacco pollen tubes with the exception of the apical dome. Within the apical PM, diffusion of both types of PM components appears to be much slower (Table 2), an effect that can perhaps be attributed to molecular crowding resulting from massive apical secretion (Goose and Sansom, 2013). To thoroughly understand apical membrane traffic underlying tip growth, the diffusion coefficients of different types of membrane components (TM proteins, FM4-64-labeled lipids) in all regions of the pollen tube PM need to be experimentally determined. To this end, photoconversion (Luo et al., 2016) along with other techniques, such as fluorescence correlation spectroscopy (Li et al., 2016) or single particle tracking (Cui et al., 2018) can be applied.

For reasons that are not entirely clear, investigating diffusion of pollen tube PM components based on regular FRAP analyses appears to be challenging. Surprisingly little recovery of PM-associated TM protein marker fluorescence was observed even after prolonged postbleach incubation within photobleached areas in subapical regions or in the shank of tobacco pollen tubes both here as well as in previously reported experiments (Lee et al., 2008). While this observation confirms that substantial secretion of the analyzed markers for membrane traffic is confined to the apical dome, it appears inconsistent with results of modeling steady-state distribution patterns of these markers, which indicate that they display typical diffusion coefficients within the PM of tobacco pollen tubes outside of the apical dome (Table 2). Photobleaching generates reactive oxygen species, including free radicals, that can damage analyzed fluorophores (Dixit and Cyr, 2003; Icha et al., 2017). Damaged TM protein markers may form stable aggregates within photobleached regions of the tobacco pollen tube PM, which possibly are highly resistant to both degeneration and penetration by freely diffusible native marker proteins present in adjacent membrane domains.

Additional Sites of Secretion and Endocytosis

Although results of the study presented here support the classical model of tip growth, suggesting that bulk secretion required for cell wall biogenesis occurs apically and is compensated by massive subapical endocytic recycling of membrane material, additional secretory and endocytic pathways with roles e.g. in the subcellular targeting or degradation of specific proteins are likely to contribute to membrane trafficking in elongating pollen tubes.

In a previous study, red-fluorescent FM4-64 labeling was analyzed by confocal time-lapse imaging during the first 10 min after dye application (redistribution stage defined in the study presented here) to tobacco pollen tubes, which already displayed steady-state labeling with preloaded FM1-43, a closely related green fluorescent styryl dye (Zonia and Munnik, 2008). Confocal images simultaneously recorded in the green and red channels were superimposed using an unspecified procedure to generate overlay images indicating regions of dye colocalization by yellow color coding. Results obtained indicated dye colocalization shortly after FM4-64 application specifically at the interface between the PM within the apical dome and apical vesicles accumulating directly underneath. As proposed by the authors, these observations may indicate that massive FM4-64 endocytosis also occurs within the apical dome of tobacco pollen tubes. However, our analysis of FM4-64 redistribution within the tobacco pollen tube PM (Fig. 1C) demonstrates that during the first 10 min after application (redistribution stage) this dye preferentially accumulates at the apex, whereas it displays a much more even distribution later at the steady-state stage. Conceivably, depending on the procedure employed, superimposition of images showing redistribution and steady-state-stage styryl dye labeling in tobacco pollen tubes (Fig. 1C), as was essentially done by Zonia and Munnik (2008), may result in overlay images similar to those presented the study published by these authors.

Bove et al. (2008) also proposed that massive endocytosis may occur at the extreme pollen tube apex based on patterns of mobility displayed by cytoplasmic components, which these authors observed at the tip of *Lilium longiflorum* pollen tubes using time-lapse differential interference contrast transmitted light microscopy as well as FRAP analysis of FM1-43-stained endomembrane compartments. Whereas the characterization and analysis of the observed mobility patterns definitely were highly informative with regards to cytoplasmic transport processes, this approach obviously can only provide indirect evidence with regards to sites of bulk endocytic PM internalization.

Visualization of the internalization of externally applied positively charged nanogold particles into tobacco pollen tubes using electron microscopy (Moscatelli et al., 2007) confirmed subapical clathrin-mediated bulk endocytic uptake of such particles, which, consistent with established FM4-64 transport routes, were either rapidly recycled to the secretory system or transported to the vacuole. However, using this technique, an additional minor pathway was identified, through which positively charged nanogold particles appear to be subapically endocytosed in a clathrin-independent manner before they are transported exclusively to the vacuole (Moscatelli et al., 2007). Interestingly, the same study also generated evidence suggesting that negatively charged nanogold particles undergo clathrin-mediated endocytosis within the apical dome rather than subapically and are also subsequently transported exclusively to the vacuole (Moscatelli et al., 2007).

Apical bulk secretion required for cell wall biogenesis at the pollen tube tip may also be complemented by additional conventional or unconventional secretory pathways (Wang et al., 2017). The vascular sorting receptor (VSR), a TM protein that typically accumulates to highest levels on the surface of endocytic endomembrane compartments, also reached the surface of tobacco pollen tubes, possibly as a consequence of temporary local fusion of prevacuolar compartments with the PM (Wang et al., 2011). Furthermore, the PME NtPPPME1, a soluble protein that is secreted at the pollen tube apex, is proposed to bypass the classical TGN on its way to the apical cell wall in tobacco pollen tubes (Wang et al., 2016).

CONCLUSION

Results of the study presented here establish that bulk secretion required for cell wall biogenesis occurs within a small apical domain (0–3.5 μm from the apex)

at the extreme tip of tobacco pollen tubes and is compensated by massive constitutive endocytic recycling, specifically of PM lipids, which is restricted to a clearly defined (5.9–14.8 μm from the apex) subapical region. The subapical F-actin fringe is not required for subapical endocytic lipid recycling but colocalizes with a detached TGN compartment, which is ideally positioned to integrate endocytic and secretory membrane traffic and to generate the secretory vesicles that are accumulating within the ARVA. Different lipid and TM protein markers for membrane traffic displayed surprisingly diverse steady distribution patterns within the pollen tube PM apparently as a consequence of marker-specific (1) rates of secretion, endocytosis, diffusion, and degradation, as well as (2) interactions with cell wall components. Together, these findings provide an essential structural basis for the characterization of molecular mechanisms responsible for the maintenance of the specific accumulation of different regulatory proteins and lipids with important functions in the control of directional cell expansion within clearly distinct domains of the PM at the tip of tobacco pollen tubes. To support and enhance results of the study presented here, it will be important to further characterize the in vivo dynamics of the investigated markers based on photoactivation or photoconversion studies, fluorescence correlation spectroscopy, and single-particle imaging.

MATERIALS AND METHODS

Plasmids

Construction and analysis of recombinant plasmid DNA (pDNA) was performed using standard methods (Snapp, 2005; Sambrook and Russell, 2012). All PCR products and junctions between ligated fragments were verified based on sequencing. For small- or large-scale pDNA purification, the mi-Plasmid miniprep kit (Metabion International) and the JetStar 2.0 maxiprep kit (Genomed) were employed, respectively.

Expression plasmids containing an eYFP complementary DNA (cDNA; BD Biosciences-Clontech) fused in frame to cDNA sequences coding for full-length or truncated forms of the following proteins were generated: tobacco (*Nicotiana tabacum*) NtINT4 (Sierro et al., 2014), Arabidopsis (*Arabidopsis thaliana*) AtRCI2a (Capel et al., 1997), AtPRK1 (Tabata et al., 2000), and Arabidopsis clathrin coat assembly protein AtAP180 (Barth and Holstein, 2004). To generate plasmids for transient expression experiments, cDNA sequences coding for NtINT4, AtPRK1, AtPRK1 lacking the first 229 N-terminal amino acids (AtPRK1ΔSP-LRR), or AtAP180 were cloned into a pUCAP-based vector (pHD32, LAT52::MCS::5×GA::eYFP::NOS; Klahre et al., 2006) using a multiple cloning site (MCS) located at the 5′ end of a cDNA encoding eYFP with a flexible 5× Gly-Ala (5×GA) linker attached at the N terminus, which was positioned between a LAT52 promoter (Twell et al., 1990) and a NOS poly(A^+) signal (derived from pBI121; Jefferson et al., 1987). The NtINT4 and AtAP180 cDNAs were inserted into this pUCAP-based vector such that the sequence encoding the 5×GA linker was eliminated. By contrast, the AtRCI2a cDNA was inserted into the MCS of another pUCAP-based vector (pWEN240, LAT52::eYFP::5×GA::MCS::NOS; Klahre et al., 2006) using a MCS located at the 3′ end of a cDNA encoding eYFP with a 5×GA linker attached at the C terminus, which was also positioned between the same LAT52 promoter and NOS poly(A^+) signal. Finally, the LAT52::NtINT4::eYFP::NOS and LAT52::eYFP::5×GA::AtRCI2a::NOS expression cassettes generated as described above were transferred into the binary vector pPZP212 (Hajdukiewicz et al., 1994) to enable stable plant transformation.

Besides the constructs cloned as indicated in the previous paragraph, additional plasmids already described in the literature were used in this study, which were also generated based on the vectors pWEN240 or pHD32 and contained between the LAT52 promoter and the NOS poly(A^+) signal cDNA sequences coding for one of the following eYFP fusion proteins: eYFP::5×GA::NtRISAP (NtRISAP, tobacco RAC5-interacting subapical pollen tube protein; Stephan et al., 2014), lifeact::5×GA::eYFP (lifeact, N-terminal 17 amino acids of yeast [*Saccharomyces cerevisiae*] actin binding protein 140 [ScAbp140$^{1–17}$]; Riedl et al., 2008; Montes-Rodriguez and Kost, 2017) and eYFP::5×GA::MTn (MTn, C-terminal 197 amino acids of mouse [*Mus musculus*] talin1 [MmTalin1$^{2345–2541}$]; Kost et al., 1998; Montes-Rodriguez and Kost, 2017). Supplemental Table S1 contains a complete list of all plasmids employed for the work presented here.

Plant Material

To establish a constant supply of fresh pollen, wild-type tobacco (Petit Havana SR1) plants were grown from seeds at regular intervals (~1 month) and maintained from seed germination to flowering in the same growth chamber under the following conditions: 16 h of illumination (200–250 μmol m^{-2} s^{-1}) at 24°C followed by 8 h of darkness at 18°C with a constant relative humidity of 60% to 65%. Seeds were germinated on sowing soil (ProfiFlor), and emerging seedlings were transferred after 2 to 3 weeks to type T soil (ProfiFlor), on which plants were subsequently grown until flowering. Fresh pollen collected from mature wild-type tobacco plants was used for all transient expression experiments. Transgenic pollen collected from transformed plants, which were grown as described above for wild-type plants, was either used fresh or was preserved by collecting mature anthers, which were immediately shock-frozen in liquid nitrogen and stored at −80°C.

Stable Plant Transformation

Transgenic tobacco plants containing LAT52::NtINT4::eYFP::NOS or LAT52::eYFP::5×GA::AtRCI2a::NOS expression cassettes were generated by *Agrobacterium tumefaciens*-mediated transformation essentially as described (Horsch and Klee, 1986). To this end, pPZP212 (Hajdukiewicz et al., 1994)-derived binary plasmids (pFAU656 or pFAU302) containing these cassettes were transformed into chemically competent *A. tumefaciens* AGL1 bacteria (Lazo et al., 1991).

Pollen Tube Culture and Transient Transformation

Fresh or preserved (at −80°C) wild-type or transgenic pollen was transferred onto "pollen tube *N. tabacum*" (PTNT) medium (Read et al., 1993a, 1993b) solidified with 0.25% (w/v) phytagel (Sigma-Aldrich) as previously described (Kost et al., 1998; Johnson and Kost, 2010). Generally, pollen collected from two to three flowers was used to prepare two 55-mm plates each containing 3.5 mL solid PTNT medium. For pollen germination and pollen tube culture, plates were placed in an incubator providing 22°C in complete darkness.

For transient transformation, immediately after plating on solid PTNT medium, wild-type pollen was bombarded with pDNA-coated gold particles using a PDS 1000/He biolistic gun (Bio-Rad) as previously described (Kost et al., 1998; Johnson and Kost, 2010). pDNA coating was performed by adding to each batch of washed particles 25 μL of 2.5 M $CaCl_2$, 10 μL of 1% (w/v) protamine sulfate (Sigma-Aldrich), and 3 μg of pDNA.

Stably or transiently transformed pollen tubes were cultured for 2.5 h before analysis by laser scanning confocal microscopy.

FM4-64 Labeling and BFA Treatment of Cultured Pollen Tubes

Stock solutions containing either 10 mM FM4-64 (Thermo Fisher Scientific) or 10 mM BFA (Thermo Fisher Scientific) in dimethyl sulfoxide (DMSO; 100% [v/v]) were prepared and stored at −20°C. FM4-64 and BFA were applied to cultured pollen tubes as described by Stephan et al. (2014). In brief, for time course imaging, 200 μL liquid PTNT medium containing 50 μM FM4-64 or 70 μM BFA was added to pollen tubes that had been growing for 2.5 h on the surface of 3.5 mL solid PTNT medium under the conditions described in the previous section. Consequently, treated pollen tubes were exposed to final concentrations of 2.7 μM FM4-64 and 0.027% (v/v) DMSO, or 3.8 μM BFA and 0.0378% (v/v) DMSO. After FM4-64 or BFA application, pollen tubes were either returned to culture or immediately imaged. Equally treated pollen tubes, to which 200 μL liquid PTNT containing just DMSO has been added (final DMSO

concentration, 0.0378% [v/v]), served as controls. For time-lapse imaging of individual pollen tubes (Supplemental Figs. S11 and S15), 200 μL liquid PTNT medium containing 15 μM FM4-64 or 50 μM BFA was added to pollen tubes growing on the surface of 3.5 mL solid PTNT medium, and samples were prepared for microscopy (as described in the next paragraph) immediately after dye or drug application.

Laser Scanning Confocal Microscopy and Growth Rate Measurement

Single-square sections (1–2.25 cm^2 in size) of solid PTNT medium were cut out with a scalpel from plates containing transformed and/or FM4-64-labeled pollen tubes, transferred onto a 76 × 26 × 1-mm glass slide and covered with a 24 × 50-mm No. 1.5 cover slip (Marienfeld Superior), which was placed directly onto the growing pollen tubes. Medial optical sections through analyzed pollen tubes were acquired using upright or inverted TCS SP5 II or SP8 DIVE-FALCON laser scanning confocal microscope (Leica Microsystems), either through an HCX PL APO CS 63.0×/1.20 NA water immersion or an HCX PL APO CS 63.0×/1.30 NA glycerol immersion objective (Leica Microsystems). Excitation at 514 nm and emission detection in the range of 525 to 565 nm or 650 to 795 nm, respectively, were employed to image eYFP and FM4-64. The same excitation and emission detection parameters were also used for simultaneous two-channel eYFP and FM4-64 imaging based on sequential line-by-line scanning. All images except those generated during FRAP experiments (see next section) were recorded with the pinhole set to a diameter of 1 Airy unit, at a resolution of 1024 × 1024 pixels and a dynamic range of 8 bit, using argon laser excitation, a scan rate of 400 Hz and 3× line averaging. Other imaging parameters (photomultiplier gain and offset, acousto-optical tunable filter transmission) were always set to maximally exploit the available dynamic range. To assess the viability of each analyzed pollen tube, its growth rate after confocal fluorescence imaging was determined by recording two time lapse images at an interval of 1 min in the transmitted light bright-field mode and by measuring the distance between the positions of the extreme pollen tube apex on the two images. ImageJ software (Abràmoff et al., 2004) was employed to import the two time lapse images and to apply a straight-line measuring tool.

FRAP

To investigate FRAP, the same hardware as described in the previous paragraph and the FRAP module of the Leica application suite advanced fluorescence image acquisition software were employed. For photobleaching, the "zoom in" and "set background to zero" functions of the FRAP module were used, and samples were exposed for four to five consecutive frames to argon laser excitation with acousto-optical tunable filter transmission set to 100% for all three laser lines (488, 496, and 514 nm). Postbleach fluorescence recovery was observed using the same imaging settings as described in the previous section with the following exceptions: time-lapse imaging was performed at a resolution of 512 × 512 pixels without line averaging. To assess the viability of each analyzed pollen tube after photobleaching, its growth rate during postbleach time-lapse imaging was determined by measuring the distance between the positions of the extreme pollen tube apex on first and the last image recorded. To this end, ImageJ software was employed as described in the previous section.

Time Lapse and Time Course Imaging

Time lapse imaging was executed by recording serial images of individual pollen tubes at regular time intervals (Fig. 2; Supplemental Figs. S2–S4, S6, S9, S11, and S15). For several reasons, time lapse imaging of pollen tubes for periods longer than a couple of minutes (Supplemental Figs. S11 and S15) represented a major challenge: (1) ambient temperature and humidity on the microscope stage gradually affected pollen tube cultures, (2) observed pollen tubes often grew against an obstacle (i.e. another pollen tube) or into the medium out of reach of high-magnification lenses with short working distances, and (3) repeated imaging of the individual pollen tube resulted in phototoxicity. These problems were largely avoided by time course imaging, which was performed without keeping track of individual pollen tubes by recording images of large numbers of different pollen tubes during each of the indicated time periods after FM4-64 or BFA application (Figs. 1C, 3A, 4A, 5, and 7; Supplemental Figs. S10 and S12). This allowed time-effective imaging of many pollen tubes under optimal conditions.

Quantitative Analysis of PM-Associated Marker Fluorescence

To quantify TM protein marker (eYFP) or FM4-64 fluorescence associated with distinct regions of the PM at different meridional distances from the extreme apex (Fig. 1, B and C, 0–32.6 μm; Fig. 2, extreme apex or center of the lateral bleached region; Figs. 3 and 4, 0–3.6 μm [Apex], 3.6–12.6 μm [Subapex], or 12.6–32.6 μm [Shank]; Supplemental Fig. S6, center of the lateral bleached region), ImageJ software (Abràmoff et al., 2004) was employed to import unprocessed confocal images and to roughly trace a segmented line with a width of 4 pixels along each membrane region to be analyzed. Subsequently, the "spline fit" function was employed to adjust the curvature of each segmented line such that it completely covered the analyzed membrane region, and a plot profile was read out providing an intensity value for each pixel of the segmented line. From these intensity values, the mean background intensity determined in a circular region of each image showing no fluorescence was subtracted. All sample and background intensity values were imported and processed using Mathematica 10.0 (Wolfram Research) or Excel software (Microsoft), respectively, to generate the line plots displayed in Figure 1, or the charts presented in Figures 2, 3, and 4, as well as in Supplemental Figure S6. Whereas line plots in Figure 1 represent absolute intensity values, Figures 2, 3, and 4, as well as Supplemental Figure S6, show normalized data. Mean intensity values obtained for the different PM regions indicated in Figures 3 and 4 were normalized for each individual imaged pollen tube to enable statistical analysis of relative levels of PM-associated marker fluorescence in the distinct regions irrespective of variability in the overall labeling intensity between different pollen tubes. To this end, the mean intensity values obtained for each pollen tube were normalized based on the highest value measured in any of the analyzed PM regions in this particular pollen tube, which was set to 100%. If possible, both sides of individual pollen tubes were separately analyzed using the described procedure, such that each pollen tube could potentially provide two independent measurements for each membrane region and time point. To quantify recovery of PM labeling in FRAP experiments, intensity values obtained for each individual analyzed pollen tube were normalized based on the prebleach value measured at the extreme apex (Fig. 2) or in the center of the lateral bleached regions (Supplemental Fig. S6), which was set to 100%.

Quantitative Analysis of the Length and Position of PM Domains

To determine the meridional distance from the extreme pollen tube apex of proximal and distal endpoints of PM domains, ImageJ software (Abràmoff et al., 2004) was employed essentially as described in the previous section. In imported images, the PM between the extreme apex and each of the two domain endpoints was roughly traced with a segmented line whose curvature was subsequently adjusted to fit the PM using the "spline fit" function. After calibration, the length of the adjusted segmented lines could be directly read out providing exact information about domain length and position. If possible, both sides of individual pollen tubes were separately analyzed as described, such that each pollen tube could potentially provide two independent measurements of the position of a membrane domain.

Statistical Analysis

Mean and SD of all data sets generated were calculated using Mathematica 10.0 (Wolfram Research; Fig. 1, line plots) or Excel software (Microsoft; all other data sets), whereas the statistical significance of differences between data sets was analyzed using GraphPad Prism software (GraphPad Software). A Student's *t*-test (Student, 1908; unpaired, parametric, and two-tailed) or ANOVA test (Fisher, 1918; parametric, nonrepeated, and one-way) was performed to assess the statistical significance of differences between the means of two or more data sets, respectively. The ANOVA Dunnett's (Dunnett, 1955) and Tukey's (Tukey, 1949) post-hocs were employed to analyze data sets with or without a reference data set, respectively. The 95% confidence level corresponding to P values of less than or equal to 0.05 (P value ≤ 0.05) was defined to indicate statistical significance.

Mathematical Modeling

The steady-state distribution profiles of TM protein markers and of FM4-64 within the pollen tube PM (Fig. 1, B and C) were mathematically expressed in the form of the following basic Fokker-Planck equations:

$$\text{TMP} \qquad D\frac{\partial^2 c(x,t)}{\partial x^2}^{\text{term 1}} - v_0\frac{\partial c(x,t)}{\partial x}^{\text{term 2}} + Q^{\text{term 3}} + Kc(x,t)^{\text{term 4}} = \frac{\partial c(x,t)}{\partial t} = 0 \qquad (1)$$

$$\text{FM4-64(apical)} \qquad D\frac{\partial^2 c(x,t)}{\partial x^2} - v_0\frac{\partial c(x,t)}{\partial x} + Q + R = \frac{\partial c(x,t)}{\partial t} = 0 \qquad (2)$$

$$\text{FM4-64(subapical)} \qquad D\frac{\partial^2 c(x,t)}{\partial x^2} - v_0\frac{\partial c(x,t)}{\partial x} + qc(x,t) + R = \frac{\partial c(x,t)}{\partial t} = 0 \qquad (3)$$

These equations define local marker concentrations $c(x,t)$ within the PM as a function of x, which is the meridional distance from the extreme pollen tube apex, and t, which represents time. $c(x,t)$ is considered proportional to the experimentally determined intensity of marker fluorescence (Soboleski et al., 2005; Lo et al., 2015). As steady-state marker distributions are modeled, $\partial c(x,t)/\partial t$ needs to equal 0. The first term of all equations accounts for marker diffusion with the coefficient D ("Results," process 3). The second term represents constant retrograde marker drift at velocity v_0, which corresponds to pollen tube growth rate and has a negative sign, as all markers drift backwards from the pollen tube apex ("Results," process 1). The third term represents local increase (source Q, positive sign, independent of marker density) or decrease (sink $qc(x,t)$, negative sign, proportional to marker density) in marker density within the PM ("Results," process 2). Finally, the fourth term represents marker degradation ($Kc(x,t)$: negative sign, proportional to marker density), or ongoing PM staining by residual FM4-64 (R, positive sign, independent of marker density; "Results," process 4).

As discussed in detail in the "Results," (1) the model divides the PM into four regions (apical a, F-actin fringe, subapical sa, shank s), and (2) the basic Fokker-Planck Equations 1 through 3 were adjusted to account for different sets of the four processes introduced in the previous paragraph occurring in each region (see Table 1), as well as to incorporate additional model assumptions. Briefly summarized, the following assumptions were made: (1) v_0 is equal in all regions, (2) in the F-actin fringe region, apart from retrograde flux, only diffusion occurs with marker-specific coefficients undergoing transition from apical to the subapical values, (3) in the shank region, $Q_s = 0$ and $q_s = 0$, (4) in the subapical region and in the shank $D_{sa} = D_s$ and $K_{sa} = K_s$, (5) in the apical dome, $K_a = 0$ and $R_a = 0$, and (6) in the subapical region, $R_{sa} = 0$. Consequently, the following modified Fokker-Planck equations were obtained, which describe TM protein marker and FM4-64 concentrations within the apical dome $c_a(x)$, the subapical region $c_{sa}(x)$, and the shank $c_s(x)$:

$$c_a(x):\ \text{TMP/FM4-64} \qquad D_a\frac{\mathrm{d}^2 c_a(x)}{\mathrm{d}x^2} - v_0\frac{\mathrm{d}c_a(x)}{\mathrm{d}x} = 0 \qquad (4)$$

$$c_{sa}(x):\ \text{TMP} \qquad D_{sa}\frac{\mathrm{d}^2 c_{sa}(x)}{\mathrm{d}x^2} - v_0\frac{\mathrm{d}c_{sa}(x)}{\mathrm{d}x} + Q_{sa} + K_{sa}c_{sa}(x) = 0 \qquad (5)$$

$$c_{sa}(x):\ \text{FM4-64} \qquad D_{sa}\frac{\mathrm{d}^2 c_{sa}(x)}{\mathrm{d}x^2} - v_0\frac{\mathrm{d}c_{sa}(x)}{\mathrm{d}x} + q_{sa}c_{sa}(x) = 0 \qquad (6)$$

$$c_s(x):\ \text{TMP} \qquad D_s\frac{\mathrm{d}^2 c_s(x)}{\mathrm{d}x^2} - v_0\frac{\mathrm{d}c_s(x)}{\mathrm{d}x} + K_s c_s(x) = 0 \qquad (7)$$

$$c_s(x):\ \text{FM4-64} \qquad D_s\frac{\mathrm{d}^2 c_s(x)}{\mathrm{d}x^2} - v_0\frac{\mathrm{d}c_s(x)}{\mathrm{d}x} + R_{sa} = 0. \qquad (8)$$

In addition, the general boundary conditions (Eqs. 9 and 10), in which a and b denote the boundary between the apical and subapical regions or between the subapical and shank regions, respectively, were applied to Equations 4 through 8 to represent the assumption that marker distribution is continuous (Eq. 9) and smooth (Eq. 10) at the borders between the four defined PM regions. Within the apical dome, Q_a was modeled as the total flux of membrane material across the border to the adjacent F-actin fringe region and hence was not directly reflected in the Fokker-Planck equations but was included in the model as a specific boundary condition for this region (Eq. 11).

$$c_a(a) = c_{sa}(a) \qquad \textit{and} \qquad c_{sa}(b) = c_s(b) \qquad (9)$$

$$\left.\frac{dc_a}{dx}\right|_{x=a} = \left.\frac{dc_{sa}}{dx}\right|_{x=a} \qquad \textit{and} \qquad \left.\frac{dc_{sa}}{dx}\right|_{x=b} = \left.\frac{dc_s}{dx}\right|_{x=b} \qquad (10)$$

$$v_0 c_a(0) - D_a\left.\frac{\mathrm{d}c_a(x)}{\mathrm{d}x}\right|_{x=0} = Q_a \qquad (11)$$

The solutions of Equations 4 to 8 reflecting all boundary conditions (Eqs. 9 to 11) and containing the constants σ, σ', $c_\infty, c_\infty', A, A', B, B', C, C'$ or E', which are defined in Supplementary Dataset S1, take the following form:

$$c_s(x):\ \text{TMP/FM4-64} \qquad c_a(x) = \frac{Q_a}{v_0} + \left(c_0 - \frac{Q_a}{v_0}\right)exp\left(\frac{v_0}{D_a}x\right) \qquad (12)$$

$$c_{sa}\ (x):\ \text{TMP} \qquad c_{sa}(x) = c_\infty - \frac{Q_{sa}}{K_{sa}} + A\ exp\left(\frac{v_0(\sigma+1)}{2D_{sa}}x\right) + B\ exp\left(-\frac{v_0(\sigma-1)}{2D_{sa}}x\right) \qquad (13)$$

$$c_{sa}\ (x):\ \text{FM4-64} \qquad c_{sa}(x) = c_\infty{}' + A'\ exp\left(\frac{v_0(\sigma'+1)}{2D_{sa}}x\right) + B'\ exp\left(\frac{v_0(\sigma'-1)}{2D_{sa}}x\right) \qquad (14)$$

$$c_s\ (x):\ \text{TMP} \qquad c_s(x) = c_\infty + C\ exp\left(-\frac{v_0(\sigma-1)}{2D_s}x\right) \qquad (15)$$

$$c_s(x):\ \text{FM4-64} \qquad c_s'(x) = \frac{R_s}{v_0}x + C'\ exp\left(\frac{v_0}{D_s}x\right) + E' \qquad (16)$$

Modeling experimental line plots displaying average intensity of PM-associated marker fluorescence (Fig. 1, B and C) required normalization of these line plots using the following equation:

$$f_i(x) = \frac{F_i(x)}{F_i(0)} = \frac{c_i(x)}{c_i(0)}, \qquad (17)$$

As discussed in detail in the results section, to optimize the fitting of solutions Equations 12 to 16 to normalized experimental data, the following marker-specific adjustments were introduced into the model: (1) for AtPRK1::eYFP, Q_{sa} was assigned the value 0 resulting in $A = 0, B = C$, and $c_{sa}(x) \rightarrow c_s(x)$. Consequently, for this marker, D_{sa} and $\sigma - 1$ in solution Equation 13 did not decouple, and the only value revealed by fitting was $\frac{\sigma-1}{D_{sa}}$; and (2) for NtINT4::eYFP, boundary condition (Eq. 10) was released, whereas boundary condition (Eq. 9) was maintained.

Fitting of the solutions (Eqs. 12 to 16) adjusted as described in the previous paragraph to the normalized experimental line plots (Fig. 8, light blue line) was performed for each marker independently using the "NonlinearModelFit" function of Mathematica 10.0 (Wolfram Research). For each marker, the three region-specific solutions were simultaneously fitted to the corresponding experimental data, such that all constants contained in these solutions could be simultaneously read out (Table 2). Because the model was fit to normalized experimental data, readout representing zeroth-order constants (Q_a, Q_{sa}, R_s) only had relative physical meaning. By contrast, readout representing diffusion coefficients (D_a, $D_{sa} = D_s$) and first-order constants ($K_s = K_{sa}$, q_{sa}) were not affected by data normalization and maintained absolute physical meaning.

Accession Numbers

The amino acid sequences of all proteins employed as markers in this study can be found in the GenBank database using the indicated accession numbers: eYFP, AAX97736; NtINT4, XP_016480732; AtRCI2a, AAD17302; AtPRK1, NP_198389; AtAP180, Q9ZVN6; NtRISAP, AHX26274; ScAbp140, AJT97542.1; and MmTalin1, NP_035732.2.

Supplemental Data

The following supplemental materials are available.

Supplemental Figure S1. Mean growth rates of tobacco pollen tubes after confocal imaging of intracellular TM protein marker distribution or of FM4-64 labeling.

Supplemental Figure S2. FRAP time lapse analysis of NtINT4::eYFP dynamics at the tip of tobacco pollen tubes.

Supplemental Figure S3. FRAP time lapse analysis of eYFP::AtRCI2a dynamics at the tip of tobacco pollen tubes.

Supplemental Figure S4. FRAP time lapse analysis of AtPRK1::eYFP dynamics at the tip of tobacco pollen tubes.

Supplemental Figure S5. Mean growth rates during postbleach time lapse imaging of tobacco pollen tubes subjected to FRAP analysis of TM protein marker dynamics at the tip.

Supplemental Figure S6. FRAP time lapse analysis of TM protein marker dynamics behind the apical dome of tobacco pollen tubes.

Supplemental Figure S7. Mean growth rates during postbleach time lapse imaging of tobacco pollen tubes subjected to FRAP analysis of TM protein marker dynamics behind the apical dome.

Supplemental Figure S8. BFA blocks tobacco pollen tube tip growth.

Supplemental Figure S9. FRAP time lapse analysis of TM protein marker dynamics at the tip of tobacco pollen tubes pretreated with BFA.

Supplemental Figure S10. Time course analysis of changes in FM4-64 labeling patterns in normally growing tobacco pollen tubes during the first 60 min after dye application.

Supplemental Figure S11. Time lapse analysis of PM labeling by different markers in individual tobacco pollen tubes.

Supplemental Figure S12. Time course analysis of BFA-induced loss of FM4-64 PM labeling in tobacco pollen tubes.

Supplemental Figure S13. Mean growth rate of tobacco pollen tubes analyzed to determine the intracellular distribution of a transiently expressed AtAP180::eYFP fusion protein.

Supplemental Figure S14. Mean growth rate of tobacco pollen tubes transiently expressing eYFP fusion proteins serving as TGN or F-actin markers at noninvasive levels.

Supplemental Figure S15. Simultaneous time-lapse analysis of FM4-64 PM labeling and of noninvasively visualized F-actin structures in individual tobacco pollen tubes treated with BFA either alone or in combination with LatB.

Supplemental Table S1. List of all plasmids used in this study.

Supplemental Data Set S1. Definition of the constants σ/σ', c_∞/c'_∞, A/A', B/B', C/C' and E' in the solutions of the Fokker-Planck equations describing marker distributions within the PM.

ACKNOWLEDGMENTS

The authors would like to thank Stephanie Scholz, Sylwia Schulmeister, Jennifer Schuster and Martin Schuster (University of Erlangen-Nuremberg) for outstanding technical support, as well as Susanne Holstein (University of Heidelberg), Chris Sommerville (University of California, Berkeley), Zhenbiao Yang (University of California, Riverside), and Norbert Sauer (University of Erlangen-Nuremberg) for providing cDNAs encoding AtAP180, AtRCI2a, AtPRK1, and NtINT4, respectively. Stefan Terjung (Advanced Light Microscopy Facility, European Molecular Biology Laboratory) and Nan Luo (University of California, Riverside) are acknowledged for invaluable help with the development of FRAP techniques employed in this study. We are also grateful for excellent scientific and technical support received from Cecilia Del Casino (University of Siena), Claudia Faleri (University of Siena), and the Optical Imaging Center Erlangen.

Received March 30, 2020; accepted May 15, 2020; published June 1, 2020.

LITERATURE CITED

Abràmoff MD, Magalhães PJ, Ram SJ (2004) Image processing with ImageJ. Biophotonics Int **11:** 36–42

Alabi AA, Tsien RW (2013) Perspectives on kiss-and-run: Role in exocytosis, endocytosis, and neurotransmission. Annu Rev Physiol **75:** 393–422

Baluska F, Hlavacka A, Samaj J, Palme K, Robinson DG, Matoh T, McCurdy DW, Menzel D, Volkmann D (2002) F-actin-dependent endocytosis of cell wall pectins in meristematic root cells. Insights from brefeldin A-induced compartments. Plant Physiol **130:** 422–431

Barth M, Holstein SE (2004) Identification and functional characterization of *Arabidopsis* AP180, a binding partner of plant alphaC-adaptin. J Cell Sci **117:** 2051–2062

Blackbourn HD, Jackson AP (1996) Plant clathrin heavy chain: Sequence analysis and restricted localisation in growing pollen tubes. J Cell Sci **109:** 777–786

Bolte S, Talbot C, Boutte Y, Catrice O, Read ND, Satiat-Jeunemaitre B (2004) FM-dyes as experimental probes for dissecting vesicle trafficking in living plant cells. J Microsc **214:** 159–173

Bosch M, Cheung AY, Hepler PK (2005) Pectin methylesterase, a regulator of pollen tube growth. Plant Physiol **138:** 1334–1346

Bosch M, Hepler PK (2005) Pectin methylesterases and pectin dynamics in pollen tubes. Plant Cell **17:** 3219–3226

Bou Daher F, Geitmann A (2011) Actin is involved in pollen tube tropism through redefining the spatial targeting of secretory vesicles. Traffic **12:** 1537–1551

Bove J, Vaillancourt B, Kroeger J, Hepler PK, Wiseman PW, Geitmann A (2008) Magnitude and direction of vesicle dynamics in growing pollen tubes using spatiotemporal image correlation spectroscopy and fluorescence recovery after photobleaching. Plant Physiol **147:** 1646–1658

Cai G, Parrotta L, Cresti M (2015) Organelle trafficking, the cytoskeleton, and pollen tube growth. J Integr Plant Biol **57:** 63–78

Capel J, Jarillo JA, Salinas J, Martínez-Zapater JM (1997) Two homologous low-temperature-inducible genes from Arabidopsis encode highly hydrophobic proteins. Plant Physiol **115:** 569–576

Cárdenas L, Lovy-Wheeler A, Kunkel JG, Hepler PK (2008) Pollen tube growth oscillations and intracellular calcium levels are reversibly modulated by actin polymerization. Plant Physiol **146:** 1611–1621

Chang F, Gu Y, Ma H, Yang Z (2013) AtPRK2 promotes ROP1 activation via RopGEFs in the control of polarized pollen tube growth. Mol Plant **6:** 1187–1201

Chebli Y, Kaneda M, Zerzour R, Geitmann A (2012) The cell wall of the Arabidopsis pollen tube—spatial distribution, recycling, and network formation of polysaccharides. Plant Physiol **160:** 1940–1955

Chen CY, Wong EI, Vidali L, Estavillo A, Hepler PK, Wu HM, Cheung AY (2002) The regulation of actin organization by actin-depolymerizing factor in elongating pollen tubes. Plant Cell **14:** 2175–2190

Cheung AY, Duan QH, Costa SS, de Graaf BH, Di Stilio VS, Feijo J, Wu HM (2008) The dynamic pollen tube cytoskeleton: Live cell studies using actin-binding and microtubule-binding reporter proteins. Mol Plant **1:** 686–702

Cheung AY, Wu HM (2007) Structural and functional compartmentalization in pollen tubes. J Exp Bot **58:** 75–82

Contento AL, Bassham DC (2012) Structure and function of endosomes in plant cells. J Cell Sci **125:** 3511–3518

Cui Y, Yu M, Yao X, Xing J, Lin J, Li X (2018) Single-particle tracking for the quantification of membrane protein dynamics in living plant cells. Mol Plant **11:** 1315–1327

Cutler SR, Ehrhardt DW, Griffitts JS, Somerville CR (2000) Random GFP: cDNA fusions enable visualization of subcellular structures in cells of *Arabidopsis* at a high frequency. Proc Natl Acad Sci USA **97:** 3718–3723

Derksen J, Rutten T, Lichtscheidl IK, de Win AHN, Pierson ES, Rongen G (1995) Quantitative analysis of the distribution of organelles in tobacco pollen tubes: Implications for exocytosis and endocytosis. Protoplasma **188:** 267–276

Dettmer J, Hong-Hermesdorf A, Stierhof YD, Schumacher K (2006) Vacuolar H+-ATPase activity is required for endocytic and secretory trafficking in Arabidopsis. Plant Cell **18:** 715–730

Dhonukshe P, Aniento F, Hwang I, Robinson DG, Mravec J, Stierhof YD, Friml J (2007) Clathrin-mediated constitutive endocytosis of PIN auxin efflux carriers in *Arabidopsis*. Curr Biol **17:** 520–527

Dixit R, Cyr R (2003) Cell damage and reactive oxygen species production induced by fluorescence microscopy: Effect on mitosis and guidelines for non-invasive fluorescence microscopy. Plant J **36:** 280–290

Dong H, Pei W, Haiyun R (2012) Actin fringe is correlated with tip growth velocity of pollen tubes. Mol Plant **5:** 1160–1162

Dowd PE, Coursol S, Skirpan AL, Kao TH, Gilroy S (2006) Petunia phospholipase c1 is involved in pollen tube growth. Plant Cell **18:** 1438–1453

Dunnett CW (1955) A multiple comparison procedure for comparing several treatments with a control. J Am Stat Assoc **50:** 1096–1121
Edidin M (1987) Rotational and lateral diffusion of membrane proteins and lipids: phenomena and function. In F Bronner, RD Klausner, C Kempf, and Jv Renswoude, eds, Current Topics in Membranes and Transport, Vol **Vol 29**. Academic Press, San Diego, CA, pp 91–127
Emans N, Zimmermann S, Fischer R (2002) Uptake of a fluorescent marker in plant cells is sensitive to brefeldin A and wortmannin. Plant Cell **14:** 71–86
Fan L, Li R, Pan J, Ding Z, Lin J (2015) Endocytosis and its regulation in plants. Trends Plant Sci **20:** 388–397
Feng Q-N, Kang H, Song S-J, Ge F-R, Zhang Y-L, Li E, Li S, Zhang Y (2016) Arabidopsis RhoGDIs are critical for cellular homeostasis of pollen tubes. Plant Physiol **170:** 841–856
Fisher R (1918) The correlation between relatives on the supposition of mendelian inheritance. Trans R Soc Edinb **52:** 399–433
Frick M, Schmidt K, Nichols BJ (2007) Modulation of lateral diffusion in the plasma membrane by protein density. Curr Biol **17:** 462–467
Fu Y, Wu G, Yang Z (2001) Rop GTPase-dependent dynamics of tip-localized F-actin controls tip growth in pollen tubes. J Cell Biol **152:** 1019–1032
Fu Y, Yang Z (2001) Rop GTPase: A master switch of cell polarity development in plants. Trends Plant Sci **6:** 545–547
Galletta BJ, Cooper JA (2009) Actin and endocytosis: Mechanisms and phylogeny. Curr Opin Cell Biol **21:** 20–27
Geitmann A, Parre E (2004) The local cytomechanical properties of growing pollen tubes correspond to the axial distribution of structural cellular elements. Sex Plant Reprod **17:** 9–16
Geldner N, Anders N, Wolters H, Keicher J, Kornberger W, Muller P, Delbarre A, Ueda T, Nakano A, Jürgens G (2003) The *Arabidopsis* GNOM ARF-GEF mediates endosomal recycling, auxin transport, and auxin-dependent plant growth. Cell **112:** 219–230
Geldner N, Friml J, Stierhof YD, Jürgens G, Palme K (2001) Auxin transport inhibitors block PIN1 cycling and vesicle trafficking. Nature **413:** 425–428
Goose JE, Sansom MSP (2013) Reduced lateral mobility of lipids and proteins in crowded membranes. PLOS Comput Biol **9:** e1003033
Grebnev G, Ntefidou M, Kost B (2017) Secretion and endocytosis in pollen tubes: Models of tip growth in the spot light. Front Plant Sci **8:** 154
Gu Y, Li S, Lord EM, Yang Z (2006) Members of a novel class of Arabidopsis Rho guanine nucleotide exchange factors control Rho GTPase-dependent polar growth. Plant Cell **18:** 366–381
Hajdukiewicz P, Svab Z, Maliga P (1994) The small, versatile *pPZP* family of *Agrobacterium* binary vectors for plant transformation. Plant Mol Biol **25:** 989–994
Hartel AJ, Glogger M, Guigas G, Jones NG, Fenz SF, Weiss M, Engstler M (2015) The molecular size of the extra-membrane domain influences the diffusion of the GPI-anchored VSG on the trypanosome plasma membrane. Sci Rep **5:** 10394
He L, Wu LG (2007) The debate on the kiss-and-run fusion at synapses. Trends Neurosci **30:** 447–455
Helling D, Possart A, Cottier S, Klahre U, Kost B (2006) Pollen tube tip growth depends on plasma membrane polarization mediated by tobacco PLC3 activity and endocytic membrane recycling. Plant Cell **18:** 3519–3534
Hepler PK, Rounds CM, Winship LJ (2013) Control of cell wall extensibility during pollen tube growth. Mol Plant **6:** 998–1017
Hepler PK, Vidali L, Cheung AY (2001) Polarized cell growth in higher plants. Annu Rev Cell Dev Biol **17:** 159–187
Horsch RB, Klee HJ (1986) Rapid assay of foreign gene expression in leaf discs transformed by *Agrobacterium tumefaciens*: Role of T-DNA borders in the transfer process. Proc Natl Acad Sci USA **83:** 4428–4432
Icha J, Weber M, Waters JC, Norden C (2017) Phototoxicity in live fluorescence microscopy, and how to avoid it. BioEssays **39:** 1700003
Jefferson RA, Kavanagh TA, Bevan MW (1987) GUS fusions: Beta-glucuronidase as a sensitive and versatile gene fusion marker in higher plants. EMBO J **6:** 3901–3907
Jiang L, Rogers JC (1998) Integral membrane protein sorting to vacuoles in plant cells: Evidence for two pathways. J Cell Biol **143:** 1183–1199
Johnson MA, Kost B (2010) Pollen tube development. Methods Mol Biol **655:** 155–176
Käll L, Krogh A, Sonnhammer EL (2007) Advantages of combined transmembrane topology and signal peptide prediction—the Phobius web server. Nucleic Acids Res **35:** W429–W432
Kaneda M, van Oostende-Triplet C, Chebli Y, Testerink C, Bednarek SY, Geitmann A (2019) Plant AP180 N-terminal homolog proteins are involved in clathrin-dependent endocytosis during pollen tube growth in *Arabidopsis thaliana*. Plant Cell Physiol **60:** 1316–1330
Ketelaar T, Galway ME, Mulder BM, Emons AM (2008) Rates of exocytosis and endocytosis in *Arabidopsis* root hairs and pollen tubes. J Microsc **231:** 265–273
Kim DH, Hwang I (2013) Direct targeting of proteins from the cytosol to organelles: The ER versus endosymbiotic organelles. Traffic **14:** 613–621
Klahre U, Becker C, Schmitt AC, Kost B (2006) Nt-RhoGDI2 regulates Rac/Rop signaling and polar cell growth in tobacco pollen tubes. Plant J **46:** 1018–1031
Klahre U, Kost B (2006) Tobacco RhoGTPase ACTIVATING PROTEIN1 spatially restricts signaling of RAC/Rop to the apex of pollen tubes. Plant Cell **18:** 3033–3046
Kost B (2008) Spatial control of Rho (Rac-Rop) signaling in tip-growing plant cells. Trends Cell Biol **18:** 119–127
Kost B, Lemichez E, Spielhofer P, Hong Y, Tolias K, Carpenter C, Chua NH (1999) Rac homologues and compartmentalized phosphatidylinositol 4, 5-bisphosphate act in a common pathway to regulate polar pollen tube growth. J Cell Biol **145:** 317–330
Kost B, Spielhofer P, Chua N-H (1998) A GFP-mouse talin fusion protein labels plant actin filaments *in vivo* and visualizes the actin cytoskeleton in growing pollen tubes. Plant J **16:** 393–401
Kusumi A, Sako Y, Yamamoto M (1993) Confined lateral diffusion of membrane receptors as studied by single particle tracking (nanovid microscopy). Effects of calcium-induced differentiation in cultured epithelial cells. Biophys J **65:** 2021–2040
Lam SK, Siu CL, Hillmer S, Jang S, An G, Robinson DG, Jiang L (2007) Rice SCAMP1 defines clathrin-coated, trans-golgi-located tubular-vesicular structures as an early endosome in tobacco BY-2 cells. Plant Cell **19:** 296–319
Lancelle SA, Hepler PK (1992) Ultrastructure of freeze-substituted pollen tubes of *Lilium longiflorum*. Protoplasma **167:** 215–230
Lazo GR, Stein PA, Ludwig RA (1991) A DNA transformation-competent *Arabidopsis* genomic library in *Agrobacterium*. Biotechnology (N Y) **9:** 963–967
Le Bail A, Schulmeister S, Perroud PF, Ntefidou M, Rensing SA, Kost B (2019) Analysis of the localization of fluorescent PpROP1 and PpROP-GEF4 fusion proteins in moss protonemata based on genomic "knock-in" and estradiol-titratable expression. Front Plant Sci **10:** 456
Lee YJ, Szumlanski A, Nielsen E, Yang Z (2008) Rho-GTPase-dependent filamentous actin dynamics coordinate vesicle targeting and exocytosis during tip growth. J Cell Biol **181:** 1155–1168
Li H, Luo N, Wang W, Liu Z, Chen J, Zhao L, Tan L, Wang C, et al (2018) The REN4 rheostat dynamically coordinates the apical and lateral domains of *Arabidopsis* pollen tubes. Nat Commun **9:** 2573
Li X, Xing J, Qiu Z, He Q, Lin J (2016) Quantification of membrane protein dynamics and interactions in plant cells by fluorescence correlation spectroscopy. Mol Plant **9:** 1229–1239
Lin Y, Wang Y, Zhu JK, Yang Z (1996) Localization of a Rho GTPase implies a role in tip growth and movement of the generative cell in pollen tubes. Plant Cell **8:** 293–303
Lippincott-Schwartz J, Yuan L, Tipper C, Amherdt M, Orci L, Klausner RD (1991) Brefeldin A's effects on endosomes, lysosomes, and the TGN suggest a general mechanism for regulating organelle structure and membrane traffic. Cell **67:** 601–616
Lo C-A, Kays I, Emran F, Lin T-J, Cvetkovska V, Chen BE (2015) Quantification of protein levels in single living cells. Cell Rep **13:** 2634–2644
Lovy-Wheeler A, Wilsen KL, Baskin TI, Hepler PK (2005) Enhanced fixation reveals the apical cortical fringe of actin filaments as a consistent feature of the pollen tube. Planta **221:** 95–104
Luo N, Yan A, Liu G, Guo J, Rong D, Kanaoka MM, Xiao Z, Xu G, Higashiyama T, Cui X, et al (2017) Exocytosis-coordinated mechanisms for tip growth underlie pollen tube growth guidance. Nat Commun **8:** 1687
Luo N, Yan A, Yang Z (2016) Measuring exocytosis rate using corrected fluorescence recovery after photoconversion. Traffic **17:** 554–564
Martinière A, Lavagi I, Nageswaran G, Rolfe DJ, Maneta-Peyret L, Luu DT, Botchway SW, Webb SED, Mongrand S, Maurel C, et al (2012)

Cell wall constrains lateral diffusion of plant plasma-membrane proteins. Proc Natl Acad Sci USA **109:** 12805–12810

McKenna ST, Kunkel JG, Bosch M, Rounds CM, Vidali L, Winship LJ, Hepler PK (2009) Exocytosis precedes and predicts the increase in growth in oscillating pollen tubes. Plant Cell **21:** 3026–3040

Medina J, Catalá R, Salinas J (2001) Developmental and stress regulation of RCI2A and RCI2B, two cold-inducible genes of Arabidopsis encoding highly conserved hydrophobic proteins. Plant Physiol **125:** 1655–1666

Meunier FA, Gutiérrez LM (2016) Captivating new roles of F-actin cortex in exocytosis and bulk endocytosis in neurosecretory cells. Trends Neurosci **39:** 605–613

Miller DD, Lancelle SA, Hepler PK (1996) Actin microfilaments do not form a dense meshwork in *Lilium longiflorum* pollen tube tips. Protoplasma **195:** 123–132

Miyawaki KN, Yang Z (2014) Extracellular signals and receptor-like kinases regulating ROP GTPases in plants. Front Plant Sci **5:** 449

Mollet JC, Leroux C, Dardelle F, Lehner A (2013) Cell wall composition, biosynthesis and remodeling during pollen tube growth. Plants (Basel) **2:** 107–147

Montes-Rodriguez A, Kost B (2017) Direct comparison of the performance of commonly employed in vivo F-actin markers (Lifeact-YFP, YFP-mTn and YFP-FABD2) in tobacco pollen tubes. Front Plant Sci **8:** 1349

Moscatelli A, Ciampolini F, Rodighiero S, Onelli E, Cresti M, Santo N, Idilli A (2007) Distinct endocytic pathways identified in tobacco pollen tubes using charged nanogold. J Cell Sci **120:** 3804–3819

Moscatelli A, Idilli AI, Rodighiero S, Caccianiga M (2012) Inhibition of actin polymerisation by low concentration Latrunculin B affects endocytosis and alters exocytosis in shank and tip of tobacco pollen tubes. Plant Biol (Stuttg) **14:** 770–782

Muro K, Matsuura-Tokita K, Tsukamoto R, Kanaoka MM, Ebine K, Higashiyama T, Nakano A, Ueda T (2018) ANTH domain-containing proteins are required for the pollen tube plasma membrane integrity via recycling ANXUR kinases. Commun Biol **1:** 152

Nebenführ A, Ritzenthaler C, Robinson DG (2002) Brefeldin A: Deciphering an enigmatic inhibitor of secretion. Plant Physiol **130:** 1102–1108

Paciorek T, Zazímalová E, Ruthardt N, Petrásek J, Stierhof YD, Kleine-Vehn J, Morris DA, Emans N, Jürgens G, Geldner N, et al (2005) Auxin inhibits endocytosis and promotes its own efflux from cells. Nature **435:** 1251–1256

Paez Valencia J, Goodman K, Otegui MS (2016) Endocytosis and endosomal trafficking in plants. Annu Rev Plant Biol **67:** 309–335

Parre E, Geitmann A (2005) Pectin and the role of the physical properties of the cell wall in pollen tube growth of *Solanum chacoense*. Planta **220:** 582–592

Parton RM, Fischer-Parton S, Trewavas AJ, Watahiki MK (2003) Pollen tubes exhibit regular periodic membrane trafficking events in the absence of apical extension. J Cell Sci **116:** 2707–2719

Parton RM, Fischer-Parton S, Watahiki MK, Trewavas AJ (2001) Dynamics of the apical vesicle accumulation and the rate of growth are related in individual pollen tubes. J Cell Sci **114:** 2685–2695

Pérez-Gómez J, Moore I (2007) Plant endocytosis: It is clathrin after all. Curr Biol **17:** R217–R219

Picton JM, Steer MW (1983) Membrane recycling and the control of secretory activity in pollen tubes. J Cell Sci **63:** 303–310

Potocký M, Pleskot R, Pejchar P, Vitale N, Kost B, Zárský V (2014) Live-cell imaging of phosphatidic acid dynamics in pollen tubes visualized by Spo20p-derived biosensor. New Phytol **203:** 483–494

Qin Y, Yang Z (2011) Rapid tip growth: Insights from pollen tubes. Semin Cell Dev Biol **22:** 816–824

Qu X, Zhang H, Xie Y, Wang J, Chen N, Huang S (2013) Arabidopsis villins promote actin turnover at pollen tube tips and facilitate the construction of actin collars. Plant Cell **25:** 1803–1817

Qu X, Zhang R, Zhang M, Diao M, Xue Y, Huang S (2017) Organizational innovation of apical actin filamtens drives rapid pollen tube growth and turning. Mol Plant **10:** 930–947

Read SM, Clarke AE, Bacic A (1993a) Requirements for division of the generative nucleus in cultured pollen tubes of *Nicotiana*. Protoplasma **174:** 101–115

Read SM, Clarke AE, Bacic A (1993b) Stimulation of growth of cultured *Nicotiana tabacum* W 38 pollen tubes by poly(ethylene glycol) and Cu(II) salts. Protoplasma **177:** 1–14

Reyes FC, Buono R, Otegui MS (2011) Plant endosomal trafficking pathways. Curr Opin Plant Biol **14:** 666–673

Riedl J, Crevenna AH, Kessenbrock K, Yu JH, Neukirchen D, Bista M, Bradke F, Jenne D, Holak TA, Werb Z, et al (2008) Lifeact: A versatile marker to visualize F-actin. Nat Methods **5:** 605–607

Röckel N, Wolf S, Kost B, Rausch T, Greiner S (2008) Elaborate spatial patterning of cell-wall PME and PMEI at the pollen tube tip involves PMEI endocytosis, and reflects the distribution of esterified and de-esterified pectins. Plant J **53:** 133–143

Rounds CM, Hepler PK, Winship LJ (2014) The apical actin fringe contributes to localized cell wall deposition and polarized growth in the lily pollen tube. Plant Physiol **166:** 139–151

Saffman PG, Delbrück M, Delbrück M (1975) Brownian motion in biological membranes. Proc Natl Acad Sci USA **72:** 3111–3113

Samaj J, Müller J, Beck M, Böhm N, Menzel D (2006) Vesicular trafficking, cytoskeleton and signalling in root hairs and pollen tubes. Trends Plant Sci **11:** 594–600

Sambrook JF, Russell DW (2012) Molecular Cloning: A Laboratory Manual, Ed 4. Cold Spring Harbor, NY, Cold Spring Harbor Laboratory Press

Schneider S, Schneidereit A, Konrad KR, Hajirezaei M-R, Gramann M, Hedrich R, Sauer N (2006) Arabidopsis INOSITOL TRANSPORTER4 mediates high-affinity H+ symport of myoinositol across the plasma membrane. Plant Physiol **141:** 565–577

Sekereš J, Pejchar P, Šantrůček J, Vukašinović N, Žárský V, Potocký M (2017) Analysis of exocyst subunit EXO70 family reveals distinct membrane polar domains in tobacco pollen tubes. Plant Physiol **173:** 1659–1675

Serna L (2005) A simple method for discriminating between cell membrane and cytosolic proteins. New Phytol **165:** 947–952

Shao S, Hegde RS (2011) Membrane protein insertion at the endoplasmic reticulum. Annu Rev Cell Dev Biol **27:** 25–56

Sierro N, Battey JN, Ouadi S, Bakaher N, Bovet L, Willig A, Goepfert S, Peitsch MC, Ivanov NV (2014) The tobacco genome sequence and its comparison with those of tomato and potato. Nat Commun **5:** 3833

Snapp E (2005) Design and use of fluorescent fusion proteins in cell biology. Curr Protoc Cell Biol **27:** 21.4.1-21.4.13

Soboleski MR, Oaks J, Halford WP (2005) Green fluorescent protein is a quantitative reporter of gene expression in individual eukaryotic cells. FASEB J **19:** 440–442

Sousa E, Kost B, Malhó R (2008) Arabidopsis phosphatidylinositol-4-monophosphate 5-kinase 4 regulates pollen tube growth and polarity by modulating membrane recycling. Plant Cell **20:** 3050–3064

Stavrou I, O'Halloran TJ (2006) The monomeric clathrin assembly protein, AP180, regulates contractile vacuole size in *Dictyostelium discoideum*. Mol Biol Cell **17:** 5381–5389

Steer MW (1989) Calcium control of pollen tube tip growth. Biol Bull **176**(2S): 18–20

Stenzel I, Ischebeck T, Quint M, Heilmann I (2012) Variable regions of PI4P 5-kinases direct PtdIns(4,5)P(2) toward alternative regulatory functions in tobacco pollen tubes. Front Plant Sci **2:** 114

Stephan O, Cottier S, Fahlén S, Montes-Rodriguez A, Sun J, Eklund DM, Klahre U, Kost B (2014) RISAP is a TGN-associated RAC5 effector regulating membrane traffic during polar cell growth in tobacco. Plant Cell **26:** 4426–4447

Student B (1908) The probable error of a mean. Biometrika **6:** 1–25

Sun J, Eklund DM, Montes-Rodriguez A, Kost B (2015) In vivo Rac/Rop localization as well as interaction with RhoGAP and RhoGDI in tobacco pollen tubes: Analysis by low-level expression of fluorescent fusion proteins and bimolecular fluorescence complementation. Plant J **84:** 83–98

Tabata S, Kaneko T, Nakamura Y, Kotani H, Kato T, Asamizu E, Miyajima N, Sasamoto S, Kimura T, Hosouchi T, et al; Kazusa DNA Research Institute; Cold Spring Harbor and Washington University in St Louis Sequencing Consortium; European Union Arabidopsis Genome Sequencing Consortium (2000) Sequence and analysis of chromosome 5 of the plant *Arabidopsis thaliana*. Nature **408:** 823–826

Thompson MV, Wolniak SM (2008) A plasma membrane-anchored fluorescent protein fusion illuminates sieve element plasma membranes in Arabidopsis and tobacco. Plant Physiol **146:** 1599–1610

Trimble WS, Grinstein S (2015) Barriers to the free diffusion of proteins and lipids in the plasma membrane. J Cell Biol **208:** 259–271

Tse YC, Lo SW, Hillmer S, Dupree P, Jiang L (2006) Dynamic response of prevacuolar compartments to brefeldin a in plant cells. Plant Physiol **142:** 1442–1459

Tukey JW (1949) Comparing individual means in the analysis of variance. Biometrics **5:** 99–114

Twell D, Yamaguchi J, McCormick S (1990) Pollen-specific gene expression in transgenic plants: Coordinate regulation of two different tomato gene promoters during microsporogenesis. Development **109:** 705–713

Uemura T (2016) Physiological roles of plant post-golgi transport pathways in membrane trafficking. Plant Cell Physiol **57:** 2013–2019

Uemura T, Nakano RT, Takagi J, Wang Y, Kramer K, Finkemeier I, Nakagami H, Tsuda K, Ueda T, Schulze-Lefert P, et al (2019) A Golgi-released subpopulation of the trans-Golgi network mediates protein secretion in Arabidopsis. Plant Physiol **179:** 519–532

van Gisbergen PAC, Esseling-Ozdoba A, Vos JW (2008) Microinjecting FM4-64 validates it as a marker of the endocytic pathway in plants. J Microsc **231:** 284–290

Vidali L, Rounds CM, Hepler PK, Bezanilla M (2009) Lifeact-mEGFP reveals a dynamic apical F-actin network in tip growing plant cells. PLoS One **4:** e5744

Viklund H, Bernsel A, Skwark M, Elofsson A (2008) SPOCTOPUS: A combined predictor of signal peptides and membrane protein topology. Bioinformatics **24:** 2928–2929

Vrljic M, Nishimura SY, Brasselet S, Moerner WE, McConnell HM (2002) Translational diffusion of individual class II MHC membrane proteins in cells. Biophys J **83:** 2681–2692

Wang H, Zhuang X, Cai Y, Cheung AY, Jiang L (2013) Apical F-actin-regulated exocytic targeting of NtPPME1 is essential for construction and rigidity of the pollen tube cell wall. Plant J **76:** 367–379

Wang H, Zhuang X, Wang X, Law AH, Zhao T, Du S, Loy MM, Jiang L (2016) A distinct pathway for polar exocytosis in plant cell wall formation. Plant Physiol **172:** 1003–1018

Wang H, Zhuang XH, Hillmer S, Robinson DG, Jiang LW (2011) Vacuolar sorting receptor (VSR) proteins reach the plasma membrane in germinating pollen tubes. Mol Plant **4:** 845–853

Wang Q, Kong L, Hao H, Wang X, Lin J, Samaj J, Baluska F (2005) Effects of brefeldin A on pollen germination and tube growth. Antagonistic effects on endocytosis and secretion. Plant Physiol **139:** 1692–1703

Wang X, Chung KP, Lin W, Jiang L (2017) Protein secretion in plants: Conventional and unconventional pathways and new techniques. J Exp Bot **69:** 21–37

Wang X, Teng Y, Wang Q, Li X, Sheng X, Zheng M, Samaj J, Baluska F, Lin J (2006) Imaging of dynamic secretory vesicles in living pollen tubes of *Picea meyeri* using evanescent wave microscopy. Plant Physiol **141:** 1591–1603

Weiß K, Neef A, Van Q, Kramer S, Gregor I, Enderlein J (2013) Quantifying the diffusion of membrane proteins and peptides in black lipid membranes with 2-focus fluorescence correlation spectroscopy. Biophys J **105:** 455–462

Wilsen KL, Lovy-Wheeler A, Voigt B, Menzel D, Kunkel JG, Hepler PK (2006) Imaging the actin cytoskeleton in growing pollen tubes. Sex Plant Reprod **19:** 51–62

Yalovsky S, Bloch D, Sorek N, Kost B (2008) Regulation of membrane trafficking, cytoskeleton dynamics, and cell polarity by ROP/RAC GTPases. Plant Physiol **147:** 1527–1543

Zárský V, Cvrcková F, Potocký M, Hála M (2009) Exocytosis and cell polarity in plants—exocyst and recycling domains. New Phytol **183:** 255–272

Zerzour R, Kroeger J, Geitmann A (2009) Polar growth in pollen tubes is associated with spatially confined dynamic changes in cell mechanical properties. Dev Biol **334:** 437–446

Zhang Y, McCormick S (2007) A distinct mechanism regulating a pollen-specific guanine nucleotide exchange factor for the small GTPase Rop in *Arabidopsis thaliana*. Proc Natl Acad Sci USA **104:** 18830–18835

Zhao XY, Wang Q, Li S, Ge FR, Zhou LZ, McCormick S, Zhang Y (2013) The juxtamembrane and carboxy-terminal domains of *Arabidopsis* PRK2 are critical for ROP-induced growth in pollen tubes. J Exp Bot **64:** 5599–5610

Zhao Y, Yan A, Feijó JA, Furutani M, Takenawa T, Hwang I, Fu Y, Yang Z (2010) Phosphoinositides regulate clathrin-dependent endocytosis at the tip of pollen tubes in Arabidopsis and tobacco. Plant Cell **22:** 4031–4044

Zonia L, Munnik T (2008) Vesicle trafficking dynamics and visualization of zones of exocytosis and endocytosis in tobacco pollen tubes. J Exp Bot **59:** 861–873